

1 **Inner retinal preservation in rat models of retinal degeneration implanted with subretinal**
2 **photovoltaic arrays**

3

4 **Jacob G. Light^{a,b}, James W. Fransen^c, Adewumi N. Adekunle^a, Alice Adkins^b, Gobinda**
5 **Pangeni^d, James Loudin^e, Keith Mathieson^{e,g}, Daniel V. Palanker^{e,f}, Maureen A. McCall^{c,d},**
6 **Machelle T. Pardue^{a,b}.**

7 ^aOphthalmology, Emory University; ^bRehab R&D Center of Excellence, Atlanta VA Medical
8 Center; ^cAnatomical Sciences & Neurobiology, ^dOphthalmology & Visual Sciences, University of
9 Louisville; ^eHansen Experimental Physics Laboratory, ^fOphthalmology, Stanford University;
10 ^gInstitute of Photonics, University of Strathclyde, UK

11

12 **Corresponding Author:**

13 Machelle T. Pardue, PhD
14 Research Service (151Oph)
15 Atlanta VA Medical Center
16 1670 Clairmont Rd
17 Decatur, GA 30033

18

19 Ph: 404-321-6111 x7342

20 Fax: 404-728-4847

21 mpardue@emory.edu

22

23

24 **Abstract:**

25 Photovoltaic arrays (PVA) implanted into the subretinal space of patients with retinitis
26 pigmentosa (RP) are designed to electrically stimulate the remaining inner retinal circuitry in
27 response to incident light, thereby recreating a visual signal when photoreceptor function
28 declines or is lost. Preservation of inner retinal circuitry is critical to the fidelity of this transmitted
29 signal to ganglion cells and beyond to higher visual targets. Post-implantation loss of retinal
30 interneurons or excessive glial scarring could diminish and/or eliminate PVA-evoked signal
31 transmission. As such, assessing the morphology of the inner retina in RP animal models with
32 subretinal PVAs is an important step in defining biocompatibility and predicting success of signal
33 transmission. In this study, we used immunohistochemical methods to qualitatively and
34 quantitatively compare inner retinal morphology after the implantation of a PVA in two RP
35 models: the Royal College of Surgeons (RCS) or transgenic S334ter-line 3 (S334ter-3)
36 rhodopsin mutant rat. Two PVA designs were compared. In the RCS rat, we implanted devices
37 in the subretinal space at 4 weeks of age and histologically examined them at 8 weeks of age
38 and found inner retinal morphology preservation with both PVA devices. In the S334ter-3 rat, we
39 implanted devices at 6 to 12 weeks of age and again, inner retinal morphology was generally
40 preserved with either PVA design 16 to 26 weeks post implantation. Specifically, the length of
41 rod bipolar cells and numbers of cholinergic amacrine cells were maintained along with their
42 characteristic inner plexiform lamination patterns. Throughout the implanted retinas we found
43 nonspecific glial reaction, but none showed additional glial scarring at the implant site. Our
44 results indicate that subretinally implanted PVAs are well-tolerated in rodent RP models and that
45 the inner retinal circuitry is preserved, consistent with our published results showing implant-
46 evoked signal transmission.

47 **Keywords:** retina, prosthetic, bipolar cells, amacrine cells, Müller glial cells

48 **1. Introduction**

49 Retinitis pigmentosa (RP) and age-related macular degeneration (AMD) are leading
50 causes of irreversible blindness worldwide (Hartong et al., 2006). In these diseases, vision loss,
51 regardless of underlying etiology, results from degeneration of retinal photoreceptors.
52 Remodeling of the inner retina occurs in late stages of disease (Jones and Marc, 2005; Marc
53 and Jones, 2003; Marc et al., 2007; Strettoi et al., 2002), but photoreceptor degeneration leaves
54 the neurons and circuitry of the inner retina relatively intact for extended periods of time
55 (Humayun et al., 1999; Jones et al., 2003; Marc and Jones, 2003; Marc et al., 2007; Strettoi et
56 al., 2002; Strettoi et al., 2003).

57 One promising approach that targets the remaining retinal circuitry to restore lost vision
58 uses prosthetic devices to functionally replace photoreceptors. Several different designs and
59 placement strategies are currently being evaluated. Epiretinal placement and stimulation of the
60 retinal ganglion cells (RGC) should require algorithms to selectively achieve information
61 transmission (Jensen et al., 2005; Humayun et al., 2012). Suprachoroidal implants (Cicione et
62 al., 2012; Kanda et al., 2004; Morimoto et al., 2011; Wong et al., 2009; Yamauchi et al., 2005)
63 and subretinal microphotodiode arrays (Chow et al., 2001; Mathieson et al., 2012; Rizzo, 2011;
64 Zrenner et al., 1999) are designed to directly stimulate bipolar cells and theoretically utilize
65 network-mediated retinal stimulation, preserving the integrative properties of second order
66 neurons in the inner plexiform layer (IPL) (Asher et al., 2007; Wang et al., 2012). Other
67 strategies utilize optogenetics to confer light sensitivity to bipolar or RGCs (Bi et al., 2006;
68 Busskamp et al., 2012; Garg and Federman, 2013; Isago et al., 2012; Lin et al., 2008; Tomita et
69 al., 2007) to directly stimulate retinal tissues.

70 Subretinally placed photovoltaic arrays (PVAs) provide targeted stimulation to the inner
71 nuclear layer (INL) (Fransen et al., 2014) due to their current density distribution and size

72 (Mathieson et al. 2012). Because bipolar cells are interneurons that connect photoreceptors to
73 RGCs they are involved in signal transmission with PVAs. Retention of these cells and
74 formation of a functional retinal-prosthetic interface would aid in visual restoration. For this to
75 occur there must be a high level of biocompatibility between the retina and prosthesis. As such,
76 measures of the integrity of the bipolar cells and other retinal constituents are critical
77 components to the evaluation of the success of any subretinal prosthetic.

78 Previous studies have attempted to characterize the condition of implanted and/or
79 electrically stimulated retinal tissue histologically and immunohistochemically (Alamusi et al.,
80 2013; Chow et al., 2001; Pardue et al., 2001; Ray et al., 2009; Ray et al., 2011; Tamaki et al.,
81 2008). However, many of these studies have examined the effects only of certain aspects of the
82 treatment paradigm, such as acute electrical stimulation or biocompatibility of a prosthetic
83 device in wild-type animals that do not exhibit degenerative pathology. In this study, we
84 examined retinal morphology after implantation of two generations of subretinal silicon devices
85 in two RP rat models. We compared a monopolar PVA (mPVA) with no perforations (Chow et
86 al., 2001) to a bipolar PVA (bPVA), which includes bipolar pixels separated by 5 μm gaps
87 (Mathieson et al., 2012). Photovoltaic pixels in monopolar devices have individual active
88 electrodes, but share a common large return electrode on the back side of the implant. Bipolar
89 pixels are composed of 3 photodiodes in series, connected between the active electrode in the
90 center of the pixel and a return electrode surrounding each pixel (Mathieson et al., 2012). All
91 devices in the present study were photoactive. The bPVA gaps enhance proximity of the
92 electrodes to inner retinal neurons and allow diffusion of extracellular milieu through the implant
93 (Adkins et al., 2013; Mathieson et al., 2012). Since the subretinal PVA stimulates retinal
94 neurons that are within close proximity to the electrode (Fransen et al., 2014), we focused our
95 analysis on inner retinal cells that are likely activated by the PVA device. Rod bipolar cells and
96 cholinergic amacrine cells represent well defined populations of cells with robust cellular

97 markers to assess overall inner retinal health. We also assessed glial reaction in tissues within
98 and distal to the implant site from 16 to 26 weeks post implantation in the S334ter-3 and 4
99 weeks post implantation in the RCS rat. Our results suggest that both the mPVA and bPVA
100 designs are well tolerated and preserve the necessary inner retinal circuitry that underlie the
101 transmission of signals to the RGCs and beyond (Fransen et al., 2014).

102 **2. Methods**

103 **2.1 Animals and Experimental Groups**

104 All animal procedures were approved by the Institutional Animal Care and Use
105 Committee and conformed to the ARVO Statement for the Use of Animals in Ophthalmology
106 and Vision Research. Two models of RP were used: the Royal College of Surgeons (RCS) and
107 S334ter-3 rats from an in-house breeding colony originated from breeders donated by Dr.
108 Matthew LaVail (University of California, San Francisco) (LaVail et al., 1975; Mullen and LaVail,
109 1976).

110 The RCS rats (n=4) were implanted binocularly at 4 weeks of age and terminated 4
111 weeks post-implantation. RCS rats exhibit a moderate rate of photoreceptor degeneration;
112 approximately 50% of the initial ONL thickness was present at the age of implantation (LaVail
113 and Battelle, 1975). Four eyes were implanted with an mPVA device and 4 with a bPVA device.
114 The eyes were divided such that all bPVA-implanted eyes were processed as frozen sections
115 for retinal cross-sections and half the mPVA eyes processed similarly with the remaining
116 prepared as retinal flat mounts.

117 S334ter-3 rats were implanted monocularly (right eye) with either an mPVA (n=4) or a
118 bPVA (n=7) from 6 to 12 weeks of age and were terminated at 22 to 32 weeks of age (16-26
119 weeks of implantation). Monocular implantation accommodated superior colliculus recordings
120 that are reported elsewhere (Fransen et al., 2014). The S334ter-3 is a rapid degeneration model

121 and most photoreceptors had degenerated at the time of implantation (McGill et al., 2012). All
122 S334ter-3 eyes were processed as frozen sections. Additional cross sections were analyzed
123 from three age-matched unimplanted control eyes from each RP strain, as well as 3 eyes from
124 8-week-old Long Evans wild-type rats acquired from Charles River.

125 **2.2 Overview of Devices**

126 Two types of PVA were explored: mPVA and bPVA (Mathieson et al., 2012; Pardue et
127 al., 2005b). mPVA devices, provided by Optobionics, Inc (Glen Ellyn, IL), were fabricated using
128 previously described thin-film fabrication methods (Chow et al., 2001). The mPVA is a 1 mm
129 diameter silicon disk, 25 μm thick, containing 1200 microphotodiodes with active electrodes on
130 one face and a common return electrode on the back, both coated with iridium oxide (Chow et
131 al., 2001). The bPVA device's photovoltaic arrays were composed of triple-diode pixels
132 fabricated on a silicon wafer. Each pixel contains an active electrode in its center and a return
133 electrode at the circumference. Upon illumination with a pulse of light, each pixel generates a bi-
134 phasic pulse of electric current flowing through the tissue between electrodes, primarily
135 stimulating the inner nuclear layer (INL) cells (Fransen et al., 2014). Electrodes were coated in
136 iridium oxide and the details of manufacturing methods of the bPVA were published previously
137 (Wang et al., 2012). Five- μm wide gaps were etched between adjacent pixels for electrical
138 isolation and to improve nutrients flow through the implant (Mathieson, et al. 2012). The bPVA
139 device measured 0.8 x 1.2 mm and was 30- μm thick. bPVA devices were left in retinal tissue for
140 histological analysis due to tissue destruction caused by removal.

141

142 **2.3 Surgical Procedure**

143 The surgical methods employed for implantation of the PVAs into the subretinal space
144 have been described previously (Pardue et al., 2005b). Briefly, rats were anesthetized

145 [ketamine (60 mg/kg) and xylazine (7.5 mg/kg)] and placed into a sterile field. A traction suture
146 was made at the superior limbus and the eye was rotated inferiorly. A ~1.0 mm incision was
147 made in the superior globe reaching the vitreous. The eye was hydrated with a drop of saline,
148 and a 10 minute waiting period was observed which allowed the retina to detach from the RPE.
149 The PVA was then slid into the subretinal space with the electrodes in contact with the retina.
150 Successful subretinal placement was confirmed via fundus examination and subsequent
151 spectral domain-ocular coherence tomography (SD-OCT) imaging (Heidelberg HRA+OCT,
152 Carlsbad, CA) (Fransen et al., 2014). Implants rested in the superior-temporal retina from 0.5 to
153 1 mm from the optic nerve head.

154 **2.4 Immunohistochemistry**

155 **2.4.1 Cross-sections**

156 Following anesthesia [ketamine (60 mg/kg)/xylazine (7.5 mg/kg)] and sacrifice [390
157 mg/mL pentobarbital sodium (Euthasol, Virbac AH, Inc., Fort Worth, TX)], eyes were
158 immediately enucleated and fixed in 4% paraformaldehyde for 30 minutes. The posterior eyecup
159 was bisected in the superior/inferior plane near the optic nerve, ensuring that the entire implant
160 was intact and present in only one of the two resulting halves (Figure 1A). mPVA devices were
161 gently extracted from the subretinal space using hydrodissection. bPVAs, which contain gaps
162 through which the retinal tissue migrates (Palanker et al., 2004), were left in place to preserve
163 retinal morphology around the implant. The tissue was cryoprotected overnight in 30% sucrose
164 in 0.1M PBS and frozen in embedding medium (O.C.T. Tissue-Tek®, Sakura Finetek, Tokyo).
165 Retinal sections in the superior/inferior plane (20-30 μ m) were cut on a cryostat and thaw-
166 mounted on glass slides. Sections containing the implant site were mounted on the same slide
167 with sections from the corresponding non-implanted half (referred to as “distal” tissue) so that
168 both sections received equal reagent exposure.

169 Table 1 lists the antibodies used, along with working dilutions and sources. Rod bipolar
170 cells were labeled with anti-protein kinase C alpha subunit (PKC α) (Kosaka et al., 1998). Müller
171 glial reaction in response to ocular stress was assessed with antibodies to glial fibrillary acidic
172 protein (GFAP) (Bringmann et al., 2006). Finally, cholinergic amacrine cells and IPL lamination
173 patterns were visualized with anti-choline acetyltransferase (ChAT) antibodies (Dijk and
174 Kamphuis, 2004). The incubation protocol has been described previously (Lee et al., 2008).
175 Briefly, following a wash in 1.0 M PBS slides were blocked for 1 hour at room temperature (10%
176 donkey serum, 1% BSA, and 1% Triton X-100 in 1.0 M PBS). Primary and secondary antibodies
177 were diluted in 1.0 M PBS containing 0.5% Triton X-100. Sections were incubated with primary
178 antibodies overnight at 4°C and secondary antibodies for 2 hours at room temperature.
179 Fluorescent secondary antibodies included donkey-anti-rabbit-DyLight® 488 (Abcam,
180 Cambridge, MA) and donkey-anti-goat-DyLight® 594 (Abcam, Cambridge, MA), both diluted
181 1:300. Sections were stained with DAPI, mounted with mounting medium (VectaShield® Hard
182 Set, Vector Laboratories, Inc., Burlingame, CA), and coverslipped.

183 Sections were visualized and images taken on a confocal microscope (Eclipse Ti
184 microscope with D-Eclipse C1 confocal controller, Nikon, Tokyo). Z-stack images spanning the
185 section thickness at 1 μ m intervals were captured using a 40 X oil immersion lens directly under
186 the implant site (“implanted”), immediately adjacent to the implant site (“adjacent”), and “distal”
187 tissue from the non-implanted portion of the eye (see Figure 1A). Images of unimplanted control
188 tissue were acquired from central, superior retinal sections. The Z-stack images were
189 condensed into max-intensity volume projections and processed using commercial software
190 (ImageJ, NIH, Bethesda, MD and Photoshop™6.0, Adobe Systems, Inc., San Jose, CA). For
191 comparisons of cross sections, extended-focus confocal images were composed of a stack of
192 26 images along the z-axis. ChAT flat mounted extended-focus confocal images were
193 comprised of a stack of 5 planes, each 1 μ m thick. Pinhole size, gain, photo multiplier, and

194 offset of the confocal microscope were standardized within experimental groups. Brightness and
195 contrast optimization was applied equally across all images, except images of GFAP-labeled
196 sections in which no optimization was performed.

197 **2.4.2 Quantification**

198 Digital confocal cross-sections were analyzed using an image program (Image J,
199 National Institute of Health, Bethesda, MA). Cross-sections of immuno-labeled S334ter-3
200 retinas, implanted with either mPVA or bPVA were quantified in the following ways: 1) the length
201 of PKC α labeled rod bipolar cells were measured from the center of the soma to the axon
202 terminals, 2) intensity of GFAP immunofluorescence was measured, and 3) the number of INL-
203 placed and displaced (in RGC layer) ChAT-positive amacrine nuclei were counted. For each
204 quantification, at least 2 sections from 2-4 retinas were analyzed. Triplicate measurements of
205 rod bipolar cells from summed z-stack PKC α -labeled images were made on each section and
206 averaged. GFAP immunoreactivity was quantified by measuring the intensity of a 55 x 40 μ m
207 region of interest (ROI) beginning at the retinal ganglion cell layer extending into the inner
208 plexiform layer and normalized to a background region without tissue of similar size. PKC α and
209 GFAP data was normalized to the distal regions to compare implant designs between different
210 ages. ChAT-labeled z-stacks were summed and the number of ChAT positive nuclei was
211 measured along a 150- μ m length on each section.

212 Statistical comparisons between mPVA and bPVA devices from each retinal region were
213 made with two-way repeated measures ANOVA using Holm-Sidak post-hoc comparisons
214 (Sigmastat v3.5 ,Systat Software, San Jose, CA).

215 **2.4.3 Flat mounts**

216 A subset of RCS eyes was processed as flat mounts, as described previously (Bernstein
217 and Guo, 2011), with the following modifications. Eyes were enucleated and fixed in 4%

218 paraformaldehyde for 2 hours. The posterior eye cups were digested in hyaluronidase (1mg/mL;
219 Sigma-Aldrich, St. Louis, MO) diluted 1:500 in 1.0 M PBS for 30 minutes. The retinas were
220 carefully dissected from the retinal pigment epithelium (RPE), washed twice in PBST (0.5%
221 Triton X-100 in 1.0M PBS), and then frozen in PBST at -80°C for 15 minutes. After thawing
222 slowly at room temperature, the retina was washed twice in PBST, blocked (10% donkey serum,
223 0.25% Triton X-100 in 1.0M PBS) for 4 hours at room temperature, and incubated in anti-ChAT
224 antibody (Table 1) overnight at 4°C. After 3 washes in PBST, donkey-anti-goat-DyLight® 594
225 secondary antibody (1:300; Abcam, Cambridge, MA) was applied for 1 hour at room
226 temperature. Following additional washes, retinas were stained with DAPI, cut into a cloverleaf
227 shape, and flattened on glass slides with the RGC layer face up. The retinas were mounted with
228 mounting medium (VectaShield® Hard Set, Vector Laboratories, Inc., Burlingame, CA) and
229 coverslipped.

230 The flat mounts were imaged using the confocal system, as described above, to
231 generate Z-stack images over the implant site and distal regions of the same retina. 3D
232 recreations were assembled and rotated using the 3D Viewer Plugin (ImageJ, NIH, Bethesda,
233 MD). Contrast and brightness were optimized equally across images (Photoshop™6.0, Adobe
234 Systems, Inc., San Jose, CA).

235 **3. Results**

236 **3.1 Rod bipolar cells maintained in both implant designs and RP models**

237 Rod bipolar cells were labeled for PKC α in both RCS and S334ter-3 rat eyes implanted
238 with either PVA design. Figure 1A shows a fundus image of an mPVA in an RCS rat and the
239 superimposed colored lines indicate the areas of the retina sampled in each of the subsequent
240 figures. Blue indicates the area within the implant site, red the area adjacent to and green the
241 area distal to the implant site.

242 Figure 1 shows representative images of PKC α positive rod bipolar cells in wild-type
243 (WT) (Figure 1B) and RCS rat retinas. An unimplanted RCS retina is shown in Figure 1F. The
244 unimplanted and the implanted RCS retinas exhibited atrophy of rod bipolar cell dendritic tufts
245 relative to WT. In implanted retinas, this was the case both within and outside implant sites. In
246 all RCS retinas, rod bipolar cells retained the other aspects of their characteristic morphology;
247 their somas were located near the outer margin of the INL and axon terminals in the distal IPL.
248 In addition, they persisted across the retina, including within the implant site regardless of
249 device design (Figure 1C, G). There were no apparent disruptions of rod bipolar cell morphology
250 between implant site, adjacent, and distal sites for both bPVA and mPVA implants (compare
251 Figure 1 C,G to D,H to E,I).

252 Implantation of subretinal devices in S334ter-3 rats had no effect on rod bipolar cell
253 morphology. Unimplanted S334ter-3 control retinas (Figure 2E) showed a complete loss of rod
254 bipolar cell dendritic arbors, disorganization of their somas, and a considerably thinner INL
255 compared to WT (Figure 2A); demonstrating a more advanced retinal degeneration compared to
256 RCS rats (Figures 1F and 2E). Similarly, S334ter-3 morphology of rod bipolar cells was
257 comparable regardless of PVA design (Figure 2B-D and 2F-H). S334ter-3 rod bipolar cells
258 retained their characteristic morphology with somas near the outer margin of the INL and axon
259 terminals in the distal IPL. In addition, there was no apparent disruption of rod bipolar cell
260 morphology between implant site, adjacent, and distal sites in the S334ter-3 rat (Figures 2B-D
261 and F-H), regardless of device design. Quantification of the length of PKC α labeled rod bipolar
262 cells in S344ter-3 rats showed no significant differences between mPVA and bPVA implanted
263 rats or retinal location (Figure 3A; Two-way repeated ANOVA, $p>0.05$).

264 **3.2 Cholinergic amacrine cells intact with implantation of PVA devices**

265 RCS and S334ter-3 sections were labeled with ChAT to explore the organization of the
266 cholinergic amacrine cells and the laminar bands that their processes form in the IPL (Figure 4).
267 The pattern of ChAT expression indicated that cholinergic amacrine cells survive within the
268 implant site and both their somas and processes maintain WT IPL lamination patterns, with cell
269 bodies in both the ganglion cell layer (GCL) and the innermost layer of the INL, and stratified
270 processes within sublaminae a and b (Figure 4). RCS and S334ter-3 tissue showed identical
271 expression patterns in unimplanted control, implanted, adjacent, and distal retinal tissue with
272 implantation of the bPVA (Figure 4B-I). mPVA-implanted retinas maintained this typical pattern
273 (data not shown). Counts of ChAT labeled nuclei in S334ter-3 eyes in both the INL and ganglion
274 cell layer had a trend towards being lower in mPVA than bPVA, but did not differ statistically
275 (Figure 3C, 3D; Two-way repeated ANOVA, $p=0.111$ and $p = 0.112$, respectively). ChAT
276 expression pattern also was examined *en face* in retinal flat mounts in a subset of RCS rats
277 (Figure 5). The general distribution of ChAT-labeled cells was consistent between control and
278 both mPVA implanted retinas for ChAT-labeled cells in both the INL and ganglion cell, which
279 tiled the retina in a mosaic fashion as expected (Figure 5A vs 5B and 5C vs 5D, respectively).

280 **3.3 Müller cell glial reaction within normal limits after implantation**

281 Glial reaction within RCS and S334ter-3 retina was evaluated using expression of GFAP
282 (Figure 6). RCS age-matched unimplanted retinas (Figure 6A) displayed strong GFAP labeling
283 in Müller glial processes that extended from the nerve fiber layer (NFL) to the partially
284 degenerated ONL. In bPVA implanted RCS retinas at 4 weeks post implantation (Figure 6B-D),
285 the glial reaction within the implant site was similar to the reaction in adjacent and distal regions;
286 we observed little to no additional glial scarring around the implant (Figure 6B). In fact, in many
287 cases, GFAP labeling appeared to be less pronounced at the implant site (Figure 6B) relative to
288 distal areas (Figure 6D). Similar results were found with mPVA devices (data not shown).

289 S334ter-3 age-matched unimplanted retinas showed intense GFAP labeling at the outer
290 edge of the INL that was not seen in RCS retina (Figure 6A, E, I). This is consistent with the
291 faster degeneration in this model and the formation of a glial seal that occurs after total
292 photoreceptor degeneration (Jones et al., 2003). While glial reaction was widespread,
293 persistent, and uniform in all S334ter-3 tissue, there was no noticeable difference in expression
294 of GFAP by Müller glia in bPVA implanted retinas adjacent or distal to the implants (Figure 6J-
295 L). Although the spatial extent of GFAP reaction was similar in mPVA implanted retinas (Figure
296 6F-H), we observed a significant increase in GFAP intensity in mPVA devices compared to
297 bPVA (Figure 3B; Two-way repeated ANOVA, main effect of device, $F(1, 15) = 14.38$, $p=0.02$;
298 Figure 3B). The differences were greatest over the implant regions with bPVA-implanted retinas
299 having less GFAP immunoreactivity.

300 **4. Discussion**

301 The use of subretinal prostheses for the restoration of vision in patients with RP or AMD
302 depends upon an intact inner retina (O'Brien et al., 2012). Thus, it is critical that implantation of
303 a subretinal device does not cause a loss of inner retinal cells or excessive gliosis/fibrosis, as
304 both would interfere with the retinal-prosthesis interface. We have shown that a functional
305 connection that requires synaptic transmission within the inner retina drives PVA evoked
306 responses in the superior colliculus (Fransen et al., 2014). Here we show that the morphological
307 basis for this connectivity is an intact inner retina in subretinally-implanted m- and bPVA
308 devices. In addition, we show that morphology is maintained in two RP rat models, one with
309 direct photoreceptor degeneration, the other with RPE dysfunction induced photoreceptor
310 degeneration. This indicates that the effect we observe is general. We assessed rod bipolar
311 cells because they represent the primary transmission pathway from the PVA to the RGCs and
312 cholinergic amacrine cells because they are one of the most numerous amacrine cells and their
313 processes form well known sublaminae in the the IPL. Together the two measures provide a

314 general assessment of inner retinal cell organization. While it is well-established that the
315 degenerating retina undergoes remodeling when all photoreceptors are lost (Gargini et al.,
316 2007; Marc et al., 2003; Strettoi et al., 2002), we show that in these models, rod bipolar cells
317 and cholinergic amacrine cells within the implant site continue to exhibit typical and well-
318 preserved morphology. Both their somata and processes within the IPL show normal
319 localization and lamination. Previous studies show that normal retinas respond to both acute
320 epiretinal electrical stimulation (Ray et al., 2009; Ray et al., 2011), or chronic subretinal
321 implantation (Chow et al., 2001; Pardue et al., 2001; Tamaki et al., 2008; Yu et al., 2009) with
322 an upregulation of GFAP expression and degenerative changes to the dendrites of rod bipolar
323 cells. One study in which photosensitive dye-coupled film was subretinally implanted into RCS
324 rat eyes showed preservation within the implant site of rod bipolar cell morphology via PKC α
325 labeling (Alamusi et al., 2013), consistent with the findings we report here.

326 The increase in GFAP labeling in all unimplanted RCS and S334ter-3 retinas compared
327 to WT (images not shown) is consistent with previous reports on retinal remodeling during
328 degeneration (Marc and Jones, 2003; Zhao et al., 2012). Importantly, GFAP labeling in and
329 around the implant site was similar to distal areas, suggesting that the glial reaction was not
330 augmented by the presence of the PVA. Previous immunohistochemical studies of subretinal
331 implants in animals with normal retinas have shown an increase in GFAP expression within the
332 implant site (Chow et al., 2001; Pardue et al., 2001; Tamaki et al., 2008; Yu et al., 2009). It is
333 feasible that any upregulation in GFAP due to implantation is masked when extensive gliosis
334 due to photoreceptor degeneration is already present. Quantification of GFAP
335 immunofluorescence showed a significant decrease in S334ter-3 retinas implanted with bPVAs
336 compared to mPVAs. This may indicate that the gap design of the bPVA is more biocompatible
337 with the retina and reduces the stress response. As the PVA devices are active and present
338 electrical current to the underlying inner retina in response to light, it is possible that GFAP

339 expression in the Müller glia is tempered by neuroprotective effects of subretinal electrical
340 stimulation, which have been characterized previously (Ciavatta et al., 2013; Pardue et al.,
341 2005a; Pardue et al., 2005b).

342 The persistence of inner retinal cells and their intact organization under the implanted
343 device are consistent with our finding that PVA evoked responses are retained in the superior
344 colliculus and require inner retinal synaptic transmission (Fransen et al., 2014). Structural
345 integrity is critical to the success of function using this subretinal approach to visual restoration.
346 The presence of normal IPL sublamination suggests that other circuits that modulate the
347 excitatory signal are retained and may provide even better RGC and central signals. When
348 translated to the clinic, implantation will be performed at mid to late stage of photoreceptor
349 degeneration, similar to the implantation stages used here in the RCS and S334ter-3 rats,
350 respectively. The morphology of the retina implanted with both PVAs was similar, which also is
351 consistent with the functional results (Fransen et al., 2014) suggesting good compatibility at
352 both stages of degeneration.

353 The development of the next-generation bPVA is intended to improve upon the design of
354 the mPVA device, which has already been implanted in human patients (Chow et al., 2010;
355 Chow et al., 2004). Bipolar design of the pixel electrodes provides much tighter confinement of
356 electric field, and appears to improve spatial resolution, compared to monopolar arrangement in
357 mPVAs (Fransen et al., 2014). Our comparisons between mPVA- and bPVA-implanted retinas
358 and the reduced glial reaction in the retinas implanted with the bPVA device with the gaps
359 between pixels suggests improved biocompatibility and may indicate a longer duration of the
360 interface between the device and the retina, which needs to be tested empirically.

361 **5. Conclusions**

362 We found that both mPVA and bPVA devices implanted into the subretinal space were
 363 well tolerated by the inner retina in two rat models of RP with regard to rod bipolar, cholinergic
 364 amacrine, and Müller cell morphology. This initial analysis could be complemented with assays
 365 of other cell types (such as cone bipolar cells, horizontal cells as well as other amacrine cell
 366 classes). Other functional analyses could be aimed at examining the RGC responses and the
 367 timing and spatial distribution of their excitatory and inhibitory inputs. With our findings this
 368 would provide a complete understanding of the morphological and functional status of the inner
 369 retina in contact with the prosthesis.

370 **Acknowledgements**

371 Funding was provided by the National Institutes of Health (R01-EY018608), the Air Force Office
 372 of Scientific Research (FA9550-04), NIH CTSA (UL1 RR025744, Stanford Spectrum fund) and a
 373 Stanford Bio-X IIP grant. K.M. was supported by an SU2P fellowship as part of an RCUK
 374 Science Bridges award. J.F. was supported by an NIH T32 grant (5 T32 HL 76138-09). M.T.P.
 375 was supported by a Research Career Scientist Award from the Department of Veterans Affairs.

376

377 **Table 1: Primary antibodies used in this study to characterize inner retinal health.**

Antigen	Antiserum	Source	Working Dilution	Cellular Target
PKC α	Polyclonal rabbit anti-PKC α	Santa Cruz Biotechnology, Inc., Dallas, TX	1:2000	Rod bipolar cells
GFAP	Polyclonal rabbit anti-GFAP	Abcam, Cambridge, MA	1:500	Glial reaction in retinal Müller cells
ChAT	Polyclonal goat anti-ChAT	Millipore, Billerica, MA	1:100	Cholinergic amacrine cells

378

379 **Figures Captions**

380 **Figure 1.** A) Sample fundus image of an RCS rat eye implanted subretinally with an mPVA.
381 White dotted line indicates location of the cut made in the superior to inferior plane bisecting the
382 posterior eye cup into implanted and non-implanted halves. “Implanted” region is indicated by
383 the blue line. The area immediately “adjacent” to the implant site is shown by the red line. The
384 green line displays an area opposite the implant within the non-implanted half, referred to as a
385 “distal” area. The implant is 1mm in diameter. PKC α labeling in retinal cross-sections from WT
386 rats (B), unimplanted control RCS rats at 2 months of age (F), RCS rats implanted from 4 to 8
387 weeks postnatal with a bPVA (C-E) and or mPVA (G-I). Rod bipolar cells are present with well-
388 preserved morphology and localization at the implant site (C and G) relative to adjacent (D and
389 H) and distal (E and I) regions. Implanted eyes show PKC α labeling consistent with that of age-
390 matched unimplanted RCS controls (F). Wild-type retinas (B) appear to exhibit more intact
391 dendritic tufts, but somata and axon terminal localization is comparable to that in RCS tissue.
392 Insets 1B, 1C, 1 F & 1G show magnified images of the dendritic tufts in the OPL. ONL=outer
393 nuclear layer, OPL=outer plexiform layer, INL=inner nuclear layer, IPL=inner plexiform layer,
394 GCL=ganglion cell layer. Scale bar=50 μ m.

395 **Figure 2.** PKC α labeling in retinal cross-sections from S334ter-3 rats implanted with a bPVA (B-
396 D, implanted from 7 to 27 weeks postnatal) or mPVA (F-H, implanted from 6 to 27 weeks
397 postnatal). Implanted sections (B and F) show rod bipolar cell morphology that is comparable to
398 that in adjacent (C and G) and distal (D and H) areas. The morphology and localization of these
399 sections is consistent with that seen in age-matched unimplanted S334ter-3 controls (E).
400 However, all S334ter-3 tissues exhibit virtually complete loss of the ONL and rod bipolar cell
401 dendrites, both of which are still evident in wild-type retina (A). Scale bar=50 μ m.

402 **Figure 3.** PKC α , GFAP, and ChAT labeling quantification. The relative length of PKC α -labeled
403 bipolar cells (A) did not show significant differences between retinal region or implant types. The
404 intensity of GFAP immunoreactivity (B) did not show significant differences between the retinal

405 location within each implant type, but did show a difference between implant types (Two-way
406 repeated ANOVA, $F(1, 15) = 14.38$ $p = 0.02$, $n = 6$). Immunoreactivity was normalized to the
407 distal position for the PKC α and GFAP labeling. ChAT immunoreactive cell counts did not show
408 significant differences between retinal location or implant type for either INL placed (C) or
409 displaced (D) cholinergic amacrine cells. Error bars represent standard error of the mean.

410 **Figure 4.** ChAT labeling in retinal cross-sections from RCS eyes (C-E, implanted from 4 to 8
411 weeks postnatal) and S334ter-3 eyes (G-I, implanted from 7 to 27 weeks postnatal) with bPVA
412 devices. Both RCS (B-E) and S334ter-3 sections (F-I), like wild-type (A), show typical
413 cholinergic amacrine cell morphology with somata in the INL and GCL and processes in a dual-
414 lamination pattern within the IPL. ChAT labeling patterns in implanted areas (C and G) are
415 identical to those in adjacent (D and H), distal (E and I), Scale bar=50 μ m.

416 **Figure 5.** ChAT-labeled retinal flat mounts from RCS rats implanted from 4 to 8 weeks postnatal
417 with an mPVA device (C and D) compared to unimplanted control eyes (A and B). *En face* view
418 of unimplanted INL placed (A) and implanted INL placed (C) ChAT positive amacrine cells
419 shows similar cholinergic amacrine cell distribution with consistent density. Similarly, labelling
420 patterns of ChAT positive amacrine cells in the ganglion cell layer were consistent between
421 unimplanted (B) and implanted (D) retinas. Scale bar=50 μ m.

422

423 **Figure 6.** GFAP labeling in retinal cross-sections from RCS (B-D) with bPVA and S334ter-3
424 eyes with mPVA (F-H) and bPVA (K-L) devices. RCS were implanted 4 to 8 weeks postnatally,
425 while the S334ter-3 animals were implanted at 12 to 32 weeks. Glial reaction is widespread in
426 all RCS tissue (A-D), but implanted areas (B) do not show increased GFAP labeling in
427 comparison with adjacent (C), distal (D), and age-matched unimplanted control (A) sections.
428 Similar to RCS tissue, S334ter-3 sections (E-L) show widespread gliosis due to photoreceptor
429 degeneration. However, GFAP labeling is not augmented in implanted regions (F and J) relative

430 to adjacent (G and K), distal (H and L), and age-matched unimplanted control section (E).
431 S334ter-3 retinas display a characteristic glial seal above the INL, not seen in wild-type retinas
432 (data not shown), consistent with advanced photoreceptor degeneration. NFL=nerve fiber layer.
433 Scale bar=50 μ m.

434

435

436

437

438

439

440

441

442

443

444

445

446

447

448

449

450

451

452

453

454

455

456 **References**

- 457 Adkins, A., Wang, W., Kaplan, H., Emery, D., Fernandez de Castro, J., Lee, S.-J., Huie, P.,
458 Palanker, D., McCall, M., Pardue, M., 2013. Morphological comparisons of flat and 3-
459 dimensional subretinal photovoltaic arrays in rat and pig models of retinitis pigmentosa.
460 Invest. Ophthalmol. Vis. Sci. 54, 1038.
- 461 Alamusi, Matsuo, T., Hosoya, O., Tsutsui, K.M., Uchida, T., 2013. Behavior tests and
462 immunohistochemical retinal response analyses in RCS rats with subretinal implantation
463 of Okayama-University-type retinal prosthesis. J. Artif. Organs 16, 343-351.
- 464 Asher, A., Segal, W.A., Baccus, S.A., Yaroslavsky, L.P., Palanker, D.V., 2007. Image
465 processing for a high-resolution optoelectronic retinal prosthesis. IEEE Trans. Biomed.
466 Eng. 54, 993-1004.
- 467 Bernstein, S.L., Guo, Y., 2011. Changes in cholinergic amacrine cells after rodent anterior
468 ischemic optic neuropathy (rAION). Invest. Ophthalmol. Vis. Sci. 52, 904-910.
- 469 Bi, A.D., Cui, J.J., Ma, Y.P., Olshevskaya, E., Pu, M.L., Dizhoor, A.M., Pan, Z.H., 2006. Ectopic
470 expression of a microbial-type rhodopsin restores visual responses in mice with
471 photoreceptor degeneration. Neuron 50, 23-33.
- 472 Bringmann, A., Pannicke, T., Grosche, J., Francke, M., Wiedemann, P., Skatchkov, S.N.,
473 Osborne, N.N., Reichenbach, A., 2006. Muller cells in the healthy and diseased retina.
474 Prog. Retin. Eye Res. 25, 397-424.
- 475 Busskamp, V., Picaud, S., Sahel, J.A., Roska, B., 2012. Optogenetic therapy for retinitis
476 pigmentosa. Gene Ther. 19, 169-175.
- 477 Chow, A.Y., Bittner, A.K., Pardue, M.T., 2010. The artificial silicon retina in retinitis pigmentosa
478 patients (an American Ophthalmological Association thesis). Trans. of the Am.
479 Ophthalmol. Soc. 108, 120-154.

480 Chow, A.Y., Chow, V.Y., Packo, K.H., Pollack, J.S., Peyman, G.A., Schuchard, R., 2004. The
481 artificial silicon retina microchip for the treatment of vision loss from retinitis pigmentosa.
482 Arch. Ophthalmol. 122, 460-469.

483 Chow, A.Y., Pardue, M.T., Chow, V.Y., Peyman, G.A., Liang, C., Perlman, J.I., Peachey, N.S.,
484 2001. Implantation of silicon chip microphotodiode arrays into the cat subretinal space.
485 IEEE Trans. Neural Syst. Rehabil. Eng. 9, 86-95.

486 Ciavatta, V.T., Mocko, J.A., Kim, M.K., Pardue, M.T., 2013. Subretinal electrical stimulation
487 preserves inner retinal function in RCS rat retina. Mol. Vis. 19, 995-1005.

488 Cicione, R., Shivdasani, M.N., Fallon, J.B., Luu, C.D., Allen, P.J., Rathbone, G.D., Shepherd,
489 R.K., Williams, C.E., 2012. Visual cortex responses to suprachoroidal electrical
490 stimulation of the retina: effects of electrode return configuration. J. Neural Eng. 9,
491 036009.

492 Dijk, F., Kamphuis, W., 2004. An immunocytochemical study on specific amacrine cell
493 subpopulations in the rat retina after ischemia. Brain Res. 1026, 205-217.

494 Fransen, J. W., Pangen, G., Pardue, M.T., McCall, M.A. 2014. Local signaling from a retinal
495 prosthetic in a rodent retinitis pigmentosa model in vivo. J. Neural Eng. 11, 046012.

496 Garg, S.J., Federman, J., 2013. Optogenetics, visual prosthesis and electrostimulation for
497 retinal dystrophies. Curr. Opin. Ophthalmol. 24, 407-414.

498 Gargini, C., Terzibasi, E., Mazzoni, F., Strettoi, E., 2007. Retinal organization in the retinal
499 degeneration 10 (rd10) mutant mouse: a morphological and ERG study. J. Comp.
500 Neurol. 500, 222-238.

501 Grünert, U., Martin, P.R., 1991. Rod bipolar cells in the macaque monkey retina:
502 immunoreactivity and connectivity. J Neurosci. 11, 2742-2758.

503 Hartong, D.T., Berson, E.L., Dryja, T.P., 2006. Retinitis pigmentosa. Lancet 368, 1795-1809.

504 Humayun, M.S., Dorn, J.D., da Cruz, L., Dagnelie, G., Sahel, J.A., Stanga, P.E., Cideciyan,
505 A.V., Duncan, J.L., Elliott, D., Filley, E., Ho, A.C., Santos, A., Safran, A.B., Arditi, A., Del

506 Priore, L.V., Greenberg, R.J., Argus, I.I.S.G., 2012. Interim results from the international
507 trial of Second Sight's visual prosthesis. *Ophthalmology* 119, 779-788.

508 Humayun, M.S., Prince, M., de Juan, E., Barron, Y., Moskowitz, M., Klock, I.B., Milam, A.H.,
509 1999. Morphometric analysis of the extramacular retina from postmortem eyes with
510 retinitis pigmentosa. *Invest. Ophthalmol. Vis. Sci.* 40, 143-148.

511 Isago, H., Sugano, E., Wang, Z., Murayama, N., Koyanagi, E., Tamai, M., Tomita, H., 2012.
512 Age-Dependent Differences in Recovered Visual Responses in Royal College of
513 Surgeons Rats Transduced with the Channelrhodopsin-2 Gene. *J. of Mol. Neurosci.* 46,
514 393-400.

515 Jensen, R.J., Ziv, O.R., Rizzo, J.F., 2005. Responses of rabbit retinal ganglion cells to electrical
516 stimulation with an epiretinal electrode. *J. Neural Eng.* 2, S16-21.

517 Jones, B.W., Watt, C.B., Frederick, J.M., Baehr, W., Chen, C.K., Levine, E.M., Milam, A.H.,
518 Lavail, M.M., Marc, R.E., 2003. Retinal remodeling triggered by photoreceptor
519 degenerations. *J. Comp. Neurol.* 464, 1-16.

520 Jones, B.W., Marc, R.E., 2005. Retinal remodeling during retinal degeneration. *Exp. Eye Res.*
521 81, 123-137.

522 Kanda, H., Morimoto, T., Fujikado, T., Tano, Y., Fukuda, Y., Sawai, H., 2004.
523 Electrophysiological studies of the feasibility of suprachoroidal-transretinal stimulation for
524 artificial vision in normal and RCS rats. *Invest. Ophthalmol. Vis. Sci.* 45, 560-566.

525 Kosaka, J., Suzuki, A., Morii, E., Nomura, S., 1998. Differential localization and expression of
526 alpha and beta isoenzymes of protein kinase C in the rat retina. *J. Neurosci. Res.* 54,
527 655-663.

528 LaVail, M.M., Battelle, B.A., 1975. Influence of eye pigmentation and light deprivation on
529 inherited retinal dystrophy in the rat. *Exp. Eye Res.* 21, 167-192.

530 LaVail, M.M., Sidman, R.L., Gerhardt, C.O., 1975. Congenic strains of RCS rats with inherited
531 retinal dystrophy. *J. Hered.* 66, 242-244.

532 Lee, E.J., Padilla, M., Merwine, D.K., Grzywacz, N.M., 2008. Developmental regulation of the
533 morphology of mouse retinal horizontal cells by visual experience. *Eur. J. Neurosci.* 27,
534 1423-1431.

535 Lin, B., Koizumi, A., Tanaka, N., Panda, S., Masland, R.H., 2008. Restoration of visual function
536 in retinal degeneration mice by ectopic expression of melanopsin. *Proc. Natl. Acad. Sci.*
537 U.S.A. 105, 16009-16014.

538 Mandel, Y., Goetz, G., Lavinsky, D., Huie, P., Mathieson, K., Wang, L., Kamins, T., Galambos,
539 L., Manivanh, R., Harris, J., Palanker, D., 2013. Cortical responses elicited by
540 photovoltaic subretinal prostheses exhibit similarities to visually evoked potentials. *Nat.*
541 *Commun.* 4, 1980.

542 Marc, R.E., Jones, B.W., 2003. Retinal remodeling in inherited photoreceptor degenerations.
543 *Mol. Neurobiol.* 28, 139-147.

544 Marc, R.E., Jones, B.W., Anderson, J.R., Kinard, K., Marshak, D.W., Wilson, J.H., Wensel, T.,
545 Lucas, R.J., 2007. Neural reprogramming in retinal degeneration. *Invest. Ophthalmol.*
546 *Vis. Sci.* 48, 3364-3371.

547 Marc, R.E., Jones, B.W., Watt, C.B., Strettoi, E., 2003. Neural remodeling in retinal
548 degeneration. *Prog. Retin. Eye Res.* 22, 607-655.

549 Mathieson, K., Loudin, J., Goetz, G., Huie, P., Wang, L., Kamins, T.I., Galambos, L., Smith, R.,
550 Harris, J.S., Sher, A., Palanker, D., 2012. Photovoltaic Retinal Prosthesis with High Pixel
551 Density. *Nat. Photonics* 6, 391-397.

552 McGill, T.J., Prusky, G.T., Douglas, R.M., Yasumura, D., Matthes, M.T., Lowe, R.J., Duncan,
553 J.L., Yang, H., Ahern, K., Daniello, K.M., Silver, B., LaVail, M.M., 2012. Discordant
554 anatomical, electrophysiological, and visual behavioral profiles of retinal degeneration in
555 rat models of retinal degenerative disease. *Invest. Ophthalmol. Vis. Sci.* 53, 6232-6244.

556 Morimoto, T., Kamei, M., Nishida, K., Sakaguchi, H., Kanda, H., Ikuno, Y., Kishima, H., Maruo,
557 T., Konoma, K., Ozawa, M., Nishida, K., Fujikado, T., 2011. Chronic Implantation of

558 Newly Developed Suprachoroidal-Transretinal Stimulation Prosthesis in Dogs. Invest.
559 Ophthalmol. Vis. Sci. 52, 6785-6792.

560 Mullen, R.J., LaVail, M.M., 1976. Inherited retinal dystrophy: primary defect in pigment
561 epithelium determined with experimental rat chimeras. Science 192, 799-801.

562 O'Brien, E.E., Greferath, U., Vessey, K.A., Jobling, A.I., Fletcher, E.L., 2012. Electronic
563 restoration of vision in those with photoreceptor degenerations. Clin. Exp. Optom. 95,
564 473-483.

565 Palanker, D., Huie, P., Vankov, A., Aramant, R., Seiler, M., Fishman, H., Marmor, M.,
566 Blumenkranz, M., 2004. Migration of retinal cells through a perforated membrane:
567 implications for a high-resolution prosthesis. Invest. Ophthalmol. Vis. Sci. 45, 3266-3270.

568 Pardue, M.T., Phillips, M.J., Yin, H., Fernandes, A., Cheng, Y., Chow, A.Y., Ball, S.L., 2005a.
569 Possible sources of neuroprotection following subretinal silicon chip implantation in RCS
570 rats. J. Neural Eng. 2, S39-47.

571 Pardue, M.T., Phillips, M.J., Yin, H., Sippy, B.D., Webb-Wood, S., Chow, A.Y., Ball, S.L., 2005b.
572 Neuroprotective effect of subretinal implants in the RCS rat. Invest. Ophthalmol. Vis. Sci.
573 46, 674-682.

574 Pardue, M.T., Stubbs, E.B., Jr., Perlman, J.I., Narfstrom, K., Chow, A.Y., Peachey, N.S., 2001.
575 Immunohistochemical studies of the retina following long-term implantation with
576 subretinal microphotodiode arrays. Exp. Eye Res. 73, 333-343.

577 Ray, A., Colodetti, L., Weiland, J.D., Hinton, D.R., Humayun, M.S., Lee, E.J., 2009.
578 Immunocytochemical analysis of retinal neurons under electrical stimulation. Brain Res.
579 1255, 89-97.

580 Ray, A., Lee, E.J., Humayun, M.S., Weiland, J.D., 2011. Continuous electrical stimulation
581 decreases retinal excitability but does not alter retinal morphology. J. Neural Eng. 8,
582 045003.

583 Rizzo, J.F., 3rd, 2011. Update on retinal prosthetic research: the Boston Retinal Implant Project.
584 J. Neuroophthalmol. 31, 160-168.

585 Strettoi, E., Porciatti, V., Falsini, B., Pignatelli, V., Rossi, C., 2002. Morphological and functional
586 abnormalities in the inner retina of the rd/rd mouse. J. Neurosci. 22, 5492-5504.

587 Strettoi, E., Pignatelli, V., Rossi, C., Porciatti, V., Falsini, B., 2003. Remodeling of second-order
588 neurons in the retina of rd/rd mutant mice. Vision Research 43, 867–877.

589 Tamaki, T., Matsuo, T., Hosoya, O., Tsutsui, K.M., Uchida, T., Okamoto, K., Uji, A., Ohtsuki, H.,
590 2008. Glial reaction to photoelectric dye-based retinal prostheses implanted in the
591 subretinal space of rats. J. Artif. Organs 11, 38-44.

592 Tomita, H., Sugano, E., Yawo, H., Ishizuka, T., Isago, H., Narikawa, S., Kugler, S., Tamai, M.,
593 2007. Restoration of visual response in aged dystrophic RCS rats using AAV-mediated
594 channelopsin-2 gene transfer. Invest. Ophthalmol. Vis. Sci. 48, 3821-3826.

595 Uji, A., Matsuo, T., Ishimaru, S., Kajiura, A., Shimamura, K., Ohtsuki, H., Dan-oh, Y., Suga, S.,
596 2005. Photoelectric dye-coupled polyethylene film as a prototype of retinal prostheses.
597 Artif. Organs 29, 53-57.

598 Wang, L., Mathieson, K., Kamins, T.I., Loudin, J.D., Galambos, L., Goetz, G., Sher, A., Mandel,
599 Y., Huie, P., Lavinsky, D., Harris, J.S., Palanker, D.V., 2012. Photovoltaic retinal
600 prosthesis: implant fabrication and performance. J. Neural Eng. 9, 046014.

601 Wong, Y.T., Chen, S.C., Seo, J.M., Morley, J.W., Lovell, N.H., Suaning, G.J., 2009. Focal
602 activation of the feline retina via a suprachoroidal electrode array. Vis. Res. 49, 825-833.

603 Yamauchi, Y., Franco, L.M., Jackson, D.J., Naber, J.F., Ziv, R.O., Rizzo, J.F., Kaplan, H.J.,
604 Enzmann, V., 2005. Comparison of electrically evoked cortical potential thresholds
605 generated with subretinal or suprachoroidal placement of a microelectrode array in the
606 rabbit. J. Neural Eng. 2, S48-56.

607 Yu, W., Wang, X., Zhao, C., Yang, Z., Dai, R., Dong, F., 2009. Biocompatibility of subretinal
608 parylene-based Ti/Pt microelectrode array in rabbit for further artificial vision studies. *J.*
609 *Ocul. Biol. Dis. Infor.* 2, 33-36.

610 Zhao, T., Li, Y., Weng, C., Yin, Z., 2012. The changes of potassium currents in RCS rat Muller
611 cell during retinal degeneration. *Brain Res.* 1427, 78-87.

612 Zrenner, E., Stett, A., Weiss, S., Aramant, R.B., Guenther, E., Kohler, K., Miliczek, K.D., Seiler,
613 M.J., Haemmerle, H., 1999. Can subretinal microphotodiodes successfully replace
614 degenerated photoreceptors? *Vis. Res.* 39, 2555-2567.

615

616

1 **Inner retinal preservation in rat models of retinal degeneration implanted with subretinal**
2 **photovoltaic arrays**

3

4 **Jacob G. Light^{a,b}, James W. Fransen^c, Adewumi N. Adekunle^a, Alice Adkins^b, Gobinda**
5 **Pangeni^d, James Loudin^e, Keith Mathieson^{e,g}, Daniel V. Palanker^{e,f}, Maureen A. McCall^{c,d},**
6 **Machelle T. Pardue^{a,b}.**

7 ^aOphthalmology, Emory University; ^bRehab R&D Center of Excellence, Atlanta VA Medical
8 Center; ^cAnatomical Sciences & Neurobiology, ^dOphthalmology & Visual Sciences, University of
9 Louisville; ^eHansen Experimental Physics Laboratory, ^fOphthalmology, Stanford University;
10 ^gInstitute of Photonics, University of Strathclyde, UK

11

12 **Corresponding Author:**

13 Machelle T. Pardue, PhD
14 Research Service (151Oph)
15 Atlanta VA Medical Center
16 1670 Clairmont Rd
17 Decatur, GA 30033

18

19 Ph: 404-321-6111 x7342

20 Fax: 404-728-4847

21 mpardue@emory.edu

22

23

24 **Abstract:**

25 Photovoltaic arrays (PVA) implanted into the subretinal space of patients with retinitis
26 pigmentosa (RP) are designed to electrically stimulate the remaining inner retinal circuitry in
27 response to incident light, thereby recreating a visual signal when photoreceptor function
28 declines or is lost. Preservation of inner retinal circuitry is critical to the fidelity of this transmitted
29 signal to ganglion cells and beyond to higher visual targets. Post-implantation loss of retinal
30 interneurons or excessive glial scarring could diminish and/or eliminate PVA-evoked signal
31 transmission. As such, assessing the morphology of the inner retina in RP animal models with
32 subretinal PVAs is an important step in defining biocompatibility and predicting success of signal
33 transmission. In this study, we used immunohistochemical methods to qualitatively and
34 quantitatively compare inner retinal morphology after the implantation of a PVA in two RP
35 models: the Royal College of Surgeons (RCS) or transgenic S334ter-line 3 (S334ter-3)
36 rhodopsin mutant rat. Two PVA designs were compared. In the RCS rat, we implanted devices
37 in the subretinal space at 4 weeks of age and histologically examined them at 8 weeks of age
38 and found inner retinal morphology preservation with both PVA devices. In the S334ter-3 rat, we
39 implanted devices at 6 to 12 weeks of age and again, inner retinal morphology was generally
40 preserved with either PVA design 16 to 26 weeks post implantation. Specifically, the length of
41 rod bipolar cells and numbers of cholinergic amacrine cells were maintained along with their
42 characteristic inner plexiform lamination patterns. Throughout the implanted retinas we found
43 nonspecific glial reaction, but none showed additional glial scarring at the implant site. Our
44 results indicate that subretinally implanted PVAs are well-tolerated in rodent RP models and that
45 the inner retinal circuitry is preserved, consistent with our published results showing implant-
46 evoked signal transmission.

47 **Keywords:** retina, prosthetic, bipolar cells, amacrine cells, Müller glial cells

48 **1. Introduction**

49 Retinitis pigmentosa (RP) and age-related macular degeneration (AMD) are leading
50 causes of irreversible blindness worldwide (Hartong et al., 2006). In these diseases, vision loss,
51 regardless of underlying etiology, results from degeneration of retinal photoreceptors.
52 Remodeling of the inner retina occurs in late stages of disease (Jones and Marc, 2005; Marc
53 and Jones, 2003; Marc et al., 2007; Strettoi et al., 2002), but photoreceptor degeneration leaves
54 the neurons and circuitry of the inner retina relatively intact for extended periods of time
55 (Humayun et al., 1999; Jones et al., 2003; Marc and Jones, 2003; Marc et al., 2007; Strettoi et
56 al., 2002; Strettoi et al., 2003).

57 One promising approach that targets the remaining retinal circuitry to restore lost vision
58 uses prosthetic devices to functionally replace photoreceptors. Several different designs and
59 placement strategies are currently being evaluated. Epiretinal placement and stimulation of the
60 retinal ganglion cells (RGC) should require algorithms to selectively achieve information
61 transmission (Jensen et al., 2005; Humayun et al., 2012). Suprachoroidal implants (Cicione et
62 al., 2012; Kanda et al., 2004; Morimoto et al., 2011; Wong et al., 2009; Yamauchi et al., 2005)
63 and subretinal microphotodiode arrays (Chow et al., 2001; Mathieson et al., 2012; Rizzo, 2011;
64 Zrenner et al., 1999) are designed to directly stimulate bipolar cells and theoretically utilize
65 network-mediated retinal stimulation, preserving the integrative properties of second order
66 neurons in the inner plexiform layer (IPL) (Asher et al., 2007; Wang et al., 2012). Other
67 strategies utilize optogenetics to confer light sensitivity to bipolar or RGCs (Bi et al., 2006;
68 Busskamp et al., 2012; Garg and Federman, 2013; Isago et al., 2012; Lin et al., 2008; Tomita et
69 al., 2007) to directly stimulate retinal tissues.

70 Subretinally placed photovoltaic arrays (PVAs) provide targeted stimulation to the inner
71 nuclear layer (INL) (Fransen et al., 2014) due to their current density distribution and size

72 (Mathieson et al. 2012). Because bipolar cells are interneurons that connect photoreceptors to
73 RGCs they are involved in signal transmission with PVAs. Retention of these cells and
74 formation of a functional retinal-prosthetic interface would aid in visual restoration. For this to
75 occur there must be a high level of biocompatibility between the retina and prosthesis. As such,
76 measures of the integrity of the bipolar cells and other retinal constituents are critical
77 components to the evaluation of the success of any subretinal prosthetic.

78 Previous studies have attempted to characterize the condition of implanted and/or
79 electrically stimulated retinal tissue histologically and immunohistochemically (Alamusi et al.,
80 2013; Chow et al., 2001; Pardue et al., 2001; Ray et al., 2009; Ray et al., 2011; Tamaki et al.,
81 2008). However, many of these studies have examined the effects only of certain aspects of the
82 treatment paradigm, such as acute electrical stimulation or biocompatibility of a prosthetic
83 device in wild-type animals that do not exhibit degenerative pathology. In this study, we
84 examined retinal morphology after implantation of two generations of subretinal silicon devices
85 in two RP rat models. We compared a monopolar PVA (mPVA) with no perforations (Chow et
86 al., 2001) to a bipolar PVA (bPVA), which includes bipolar pixels separated by 5 μm gaps
87 (Mathieson et al., 2012). Photovoltaic pixels in monopolar devices have individual active
88 electrodes, but share a common large return electrode on the back side of the implant. Bipolar
89 pixels are composed of 3 photodiodes in series, connected between the active electrode in the
90 center of the pixel and a return electrode surrounding each pixel (Mathieson et al., 2012). All
91 devices in the present study were photoactive. The bPVA gaps enhance proximity of the
92 electrodes to inner retinal neurons and allow diffusion of extracellular milieu through the implant
93 (Adkins et al., 2013; Mathieson et al., 2012). Since the subretinal PVA stimulates retinal
94 neurons that are within close proximity to the electrode (Fransen et al., 2014), we focused our
95 analysis on inner retinal cells that are likely activated by the PVA device. Rod bipolar cells and
96 cholinergic amacrine cells represent well defined populations of cells with robust cellular

97 markers to assess overall inner retinal health. We also assessed glial reaction in tissues within
98 and distal to the implant site from 16 to 26 weeks post implantation in the S334ter-3 and 4
99 weeks post implantation in the RCS rat. Our results suggest that both the mPVA and bPVA
100 designs are well tolerated and preserve the necessary inner retinal circuitry that underlie the
101 transmission of signals to the RGCs and beyond (Fransen et al., 2014).

102 **2. Methods**

103 **2.1 Animals and Experimental Groups**

104 All animal procedures were approved by the Institutional Animal Care and Use
105 Committee and conformed to the ARVO Statement for the Use of Animals in Ophthalmology
106 and Vision Research. Two models of RP were used: the Royal College of Surgeons (RCS) and
107 S334ter-3 rats from an in-house breeding colony originated from breeders donated by Dr.
108 Matthew LaVail (University of California, San Francisco) (LaVail et al., 1975; Mullen and LaVail,
109 1976).

110 The RCS rats (n=4) were implanted binocularly at 4 weeks of age and terminated 4
111 weeks post-implantation. RCS rats exhibit a moderate rate of photoreceptor degeneration;
112 approximately 50% of the initial ONL thickness was present at the age of implantation (LaVail
113 and Battelle, 1975). Four eyes were implanted with an mPVA device and 4 with a bPVA device.
114 The eyes were divided such that all bPVA-implanted eyes were processed as frozen sections
115 for retinal cross-sections and half the mPVA eyes processed similarly with the remaining
116 prepared as retinal flat mounts.

117 S334ter-3 rats were implanted monocularly (right eye) with either an mPVA (n=4) or a
118 bPVA (n=7) from 6 to 12 weeks of age and were terminated at 22 to 32 weeks of age (16-26
119 weeks of implantation). Monocular implantation accommodated superior colliculus recordings
120 that are reported elsewhere (Fransen et al., 2014). The S334ter-3 is a rapid degeneration model

121 and most photoreceptors had degenerated at the time of implantation (McGill et al., 2012). All
122 S334ter-3 eyes were processed as frozen sections. Additional cross sections were analyzed
123 from three age-matched unimplanted control eyes from each RP strain, as well as 3 eyes from
124 8-week-old Long Evans wild-type rats acquired from Charles River.

125 **2.2 Overview of Devices**

126 Two types of PVA were explored: mPVA and bPVA (Mathieson et al., 2012; Pardue et
127 al., 2005b). mPVA devices, provided by Optobionics, Inc (Glen Ellyn, IL), were fabricated using
128 previously described thin-film fabrication methods (Chow et al., 2001). The mPVA is a 1 mm
129 diameter silicon disk, 25 μm thick, containing 1200 microphotodiodes with active electrodes on
130 one face and a common return electrode on the back, both coated with iridium oxide (Chow et
131 al., 2001). The bPVA device's photovoltaic arrays were composed of triple-diode pixels
132 fabricated on a silicon wafer. Each pixel contains an active electrode in its center and a return
133 electrode at the circumference. Upon illumination with a pulse of light, each pixel generates a bi-
134 phasic pulse of electric current flowing through the tissue between electrodes, primarily
135 stimulating the inner nuclear layer (INL) cells (Fransen et al., 2014). Electrodes were coated in
136 iridium oxide and the details of manufacturing methods of the bPVA were published previously
137 (Wang et al., 2012). Five- μm wide gaps were etched between adjacent pixels for electrical
138 isolation and to improve nutrients flow through the implant (Mathieson, et al. 2012). The bPVA
139 device measured 0.8 x 1.2 mm and was 30- μm thick. bPVA devices were left in retinal tissue for
140 histological analysis due to tissue destruction caused by removal.

141

142 **2.3 Surgical Procedure**

143 The surgical methods employed for implantation of the PVAs into the subretinal space
144 have been described previously (Pardue et al., 2005b). Briefly, rats were anesthetized

145 [ketamine (60 mg/kg) and xylazine (7.5 mg/kg)] and placed into a sterile field. A traction suture
146 was made at the superior limbus and the eye was rotated inferiorly. A ~1.0 mm incision was
147 made in the superior globe reaching the vitreous. The eye was hydrated with a drop of saline,
148 and a 10 minute waiting period was observed which allowed the retina to detach from the RPE.
149 The PVA was then slid into the subretinal space with the electrodes in contact with the retina.
150 Successful subretinal placement was confirmed via fundus examination and subsequent
151 spectral domain-ocular coherence tomography (SD-OCT) imaging (Heidelberg HRA+OCT,
152 Carlsbad, CA) (Fransen et al., 2014). Implants rested in the superior-temporal retina from 0.5 to
153 1 mm from the optic nerve head.

154 **2.4 Immunohistochemistry**

155 **2.4.1 Cross-sections**

156 Following anesthesia [ketamine (60 mg/kg)/xylazine (7.5 mg/kg)] and sacrifice [390
157 mg/mL pentobarbital sodium (Euthasol, Virbac AH, Inc., Fort Worth, TX)], eyes were
158 immediately enucleated and fixed in 4% paraformaldehyde for 30 minutes. The posterior eyecup
159 was bisected in the superior/inferior plane near the optic nerve, ensuring that the entire implant
160 was intact and present in only one of the two resulting halves (Figure 1A). mPVA devices were
161 gently extracted from the subretinal space using hydrodissection. bPVAs, which contain gaps
162 through which the retinal tissue migrates (Palanker et al., 2004), were left in place to preserve
163 retinal morphology around the implant. The tissue was cryoprotected overnight in 30% sucrose
164 in 0.1M PBS and frozen in embedding medium (O.C.T. Tissue-Tek®, Sakura Finetek, Tokyo).
165 Retinal sections in the superior/inferior plane (20-30 μ m) were cut on a cryostat and thaw-
166 mounted on glass slides. Sections containing the implant site were mounted on the same slide
167 with sections from the corresponding non-implanted half (referred to as “distal” tissue) so that
168 both sections received equal reagent exposure.

169 Table 1 lists the antibodies used, along with working dilutions and sources. Rod bipolar
170 cells were labeled with anti-protein kinase C alpha subunit (PKC α) (Kosaka et al., 1998). Müller
171 glial reaction in response to ocular stress was assessed with antibodies to glial fibrillary acidic
172 protein (GFAP) (Bringmann et al., 2006). Finally, cholinergic amacrine cells and IPL lamination
173 patterns were visualized with anti-choline acetyltransferase (ChAT) antibodies (Dijk and
174 Kamphuis, 2004). The incubation protocol has been described previously (Lee et al., 2008).
175 Briefly, following a wash in 1.0 M PBS slides were blocked for 1 hour at room temperature (10%
176 donkey serum, 1% BSA, and 1% Triton X-100 in 1.0 M PBS). Primary and secondary antibodies
177 were diluted in 1.0 M PBS containing 0.5% Triton X-100. Sections were incubated with primary
178 antibodies overnight at 4°C and secondary antibodies for 2 hours at room temperature.
179 Fluorescent secondary antibodies included donkey-anti-rabbit-DyLight® 488 (Abcam,
180 Cambridge, MA) and donkey-anti-goat-DyLight® 594 (Abcam, Cambridge, MA), both diluted
181 1:300. Sections were stained with DAPI, mounted with mounting medium (VectaShield® Hard
182 Set, Vector Laboratories, Inc., Burlingame, CA), and coverslipped.

183 Sections were visualized and images taken on a confocal microscope (Eclipse Ti
184 microscope with D-Eclipse C1 confocal controller, Nikon, Tokyo). Z-stack images spanning the
185 section thickness at 1 μ m intervals were captured using a 40 X oil immersion lens directly under
186 the implant site (“implanted”), immediately adjacent to the implant site (“adjacent”), and “distal”
187 tissue from the non-implanted portion of the eye (see Figure 1A). Images of unimplanted control
188 tissue were acquired from central, superior retinal sections. The Z-stack images were
189 condensed into max-intensity volume projections and processed using commercial software
190 (ImageJ, NIH, Bethesda, MD and Photoshop™6.0, Adobe Systems, Inc., San Jose, CA). For
191 comparisons of cross sections, extended-focus confocal images were composed of a stack of
192 26 images along the z-axis. ChAT flat mounted extended-focus confocal images were
193 comprised of a stack of 5 planes, each 1 μ m thick. Pinhole size, gain, photo multiplier, and

194 offset of the confocal microscope were standardized within experimental groups. Brightness and
195 contrast optimization was applied equally across all images, except images of GFAP-labeled
196 sections in which no optimization was performed.

197 **2.4.2 Quantification**

198 Digital confocal cross-sections were analyzed using an image program (Image J,
199 National Institute of Health, Bethesda, MA). Cross-sections of immuno-labeled S334ter-3
200 retinas, implanted with either mPVA or bPVA were quantified in the following ways: 1) the length
201 of PKC α labeled rod bipolar cells were measured from the center of the soma to the axon
202 terminals, 2) intensity of GFAP immunofluorescence was measured, and 3) the number of INL-
203 placed and displaced (in RGC layer) ChAT-positive amacrine nuclei were counted. For each
204 quantification, at least 2 sections from 2-4 retinas were analyzed. Triplicate measurements of
205 rod bipolar cells from summed z-stack PKC α -labeled images were made on each section and
206 averaged. GFAP immunoreactivity was quantified by measuring the intensity of a 55 x 40 μ m
207 region of interest (ROI) beginning at the retinal ganglion cell layer extending into the inner
208 plexiform layer and normalized to a background region without tissue of similar size. PKC α and
209 GFAP data was normalized to the distal regions to compare implant designs between different
210 ages. ChAT-labeled z-stacks were summed and the number of ChAT positive nuclei was
211 measured along a 150- μ m length on each section.

212 Statistical comparisons between mPVA and bPVA devices from each retinal region were
213 made with two-way repeated measures ANOVA using Holm-Sidak post-hoc comparisons
214 (Sigmastat v3.5 ,Systat Software, San Jose, CA).

215 **2.4.3 Flat mounts**

216 A subset of RCS eyes was processed as flat mounts, as described previously (Bernstein
217 and Guo, 2011), with the following modifications. Eyes were enucleated and fixed in 4%

218 paraformaldehyde for 2 hours. The posterior eye cups were digested in hyaluronidase (1mg/mL;
219 Sigma-Aldrich, St. Louis, MO) diluted 1:500 in 1.0 M PBS for 30 minutes. The retinas were
220 carefully dissected from the retinal pigment epithelium (RPE), washed twice in PBST (0.5%
221 Triton X-100 in 1.0M PBS), and then frozen in PBST at -80°C for 15 minutes. After thawing
222 slowly at room temperature, the retina was washed twice in PBST, blocked (10% donkey serum,
223 0.25% Triton X-100 in 1.0M PBS) for 4 hours at room temperature, and incubated in anti-ChAT
224 antibody (Table 1) overnight at 4°C. After 3 washes in PBST, donkey-anti-goat-DyLight® 594
225 secondary antibody (1:300; Abcam, Cambridge, MA) was applied for 1 hour at room
226 temperature. Following additional washes, retinas were stained with DAPI, cut into a cloverleaf
227 shape, and flattened on glass slides with the RGC layer face up. The retinas were mounted with
228 mounting medium (VectaShield® Hard Set, Vector Laboratories, Inc., Burlingame, CA) and
229 coverslipped.

230 The flat mounts were imaged using the confocal system, as described above, to
231 generate Z-stack images over the implant site and distal regions of the same retina. 3D
232 recreations were assembled and rotated using the 3D Viewer Plugin (ImageJ, NIH, Bethesda,
233 MD). Contrast and brightness were optimized equally across images (Photoshop™6.0, Adobe
234 Systems, Inc., San Jose, CA).

235 **3. Results**

236 **3.1 Rod bipolar cells maintained in both implant designs and RP models**

237 Rod bipolar cells were labeled for PKC α in both RCS and S334ter-3 rat eyes implanted
238 with either PVA design. Figure 1A shows a fundus image of an mPVA in an RCS rat and the
239 superimposed colored lines indicate the areas of the retina sampled in each of the subsequent
240 figures. Blue indicates the area within the implant site, red the area adjacent to and green the
241 area distal to the implant site.

242 Figure 1 shows representative images of PKC α positive rod bipolar cells in wild-type
243 (WT) (Figure 1B) and RCS rat retinas. An unimplanted RCS retina is shown in Figure 1F. The
244 unimplanted and the implanted RCS retinas exhibited atrophy of rod bipolar cell dendritic tufts
245 relative to WT. In implanted retinas, this was the case both within and outside implant sites. In
246 all RCS retinas, rod bipolar cells retained the other aspects of their characteristic morphology;
247 their somas were located near the outer margin of the INL and axon terminals in the distal IPL.
248 In addition, they persisted across the retina, including within the implant site regardless of
249 device design (Figure 1C, G). There were no apparent disruptions of rod bipolar cell morphology
250 between implant site, adjacent, and distal sites for both bPVA and mPVA implants (compare
251 Figure 1 C,G to D,H to E,I).

252 Implantation of subretinal devices in S334ter-3 rats had no effect on rod bipolar cell
253 morphology. Unimplanted S334ter-3 control retinas (Figure 2E) showed a complete loss of rod
254 bipolar cell dendritic arbors, disorganization of their somas, and a considerably thinner INL
255 compared to WT (Figure 2A); demonstrating a more advanced retinal degeneration compared to
256 RCS rats (Figures 1F and 2E). Similarly, S334ter-3 morphology of rod bipolar cells was
257 comparable regardless of PVA design (Figure 2B-D and 2F-H). S334ter-3 rod bipolar cells
258 retained their characteristic morphology with somas near the outer margin of the INL and axon
259 terminals in the distal IPL. In addition, there was no apparent disruption of rod bipolar cell
260 morphology between implant site, adjacent, and distal sites in the S334ter-3 rat (Figures 2B-D
261 and F-H), regardless of device design. Quantification of the length of PKC α labeled rod bipolar
262 cells in S344ter-3 rats showed no significant differences between mPVA and bPVA implanted
263 rats or retinal location (Figure 3A; Two-way repeated ANOVA, $p > 0.05$).

264 **3.2 Cholinergic amacrine cells intact with implantation of PVA devices**

265 RCS and S334ter-3 sections were labeled with ChAT to explore the organization of the
266 cholinergic amacrine cells and the laminar bands that their processes form in the IPL (Figure 4).
267 The pattern of ChAT expression indicated that cholinergic amacrine cells survive within the
268 implant site and both their somas and processes maintain WT IPL lamination patterns, with cell
269 bodies in both the ganglion cell layer (GCL) and the innermost layer of the INL, and stratified
270 processes within sublaminae a and b (Figure 4). RCS and S334ter-3 tissue showed identical
271 expression patterns in unimplanted control, implanted, adjacent, and distal retinal tissue with
272 implantation of the bPVA (Figure 4B-I). mPVA-implanted retinas maintained this typical pattern
273 (data not shown). Counts of ChAT labeled nuclei in S334ter-3 eyes in both the INL and ganglion
274 cell layer had a trend towards being lower in mPVA than bPVA, but did not differ statistically
275 (Figure 3C, 3D; Two-way repeated ANOVA, $p=0.111$ and $p = 0.112$, respectively). ChAT
276 expression pattern also was examined *en face* in retinal flat mounts in a subset of RCS rats
277 (Figure 5). The general distribution of ChAT-labeled cells was consistent between control and
278 both mPVA implanted retinas for ChAT-labeled cells in both the INL and ganglion cell, which
279 tiled the retina in a mosaic fashion as expected (Figure 5A vs 5B and 5C vs 5D, respectively).

280 **3.3 Müller cell glial reaction within normal limits after implantation**

281 Glial reaction within RCS and S334ter-3 retina was evaluated using expression of GFAP
282 (Figure 6). RCS age-matched unimplanted retinas (Figure 6A) displayed strong GFAP labeling
283 in Müller glial processes that extended from the nerve fiber layer (NFL) to the partially
284 degenerated ONL. In bPVA implanted RCS retinas at 4 weeks post implantation (Figure 6B-D),
285 the glial reaction within the implant site was similar to the reaction in adjacent and distal regions;
286 we observed little to no additional glial scarring around the implant (Figure 6B). In fact, in many
287 cases, GFAP labeling appeared to be less pronounced at the implant site (Figure 6B) relative to
288 distal areas (Figure 6D). Similar results were found with mPVA devices (data not shown).

289 S334ter-3 age-matched unimplanted retinas showed intense GFAP labeling at the outer
290 edge of the INL that was not seen in RCS retina (Figure 6A, E, I). This is consistent with the
291 faster degeneration in this model and the formation of a glial seal that occurs after total
292 photoreceptor degeneration (Jones et al., 2003). While glial reaction was widespread,
293 persistent, and uniform in all S334ter-3 tissue, there was no noticeable difference in expression
294 of GFAP by Müller glia in bPVA implanted retinas adjacent or distal to the implants (Figure 6J-
295 L). Although the spatial extent of GFAP reaction was similar in mPVA implanted retinas (Figure
296 6F-H), we observed a significant increase in GFAP intensity in mPVA devices compared to
297 bPVA (Figure 3B; Two-way repeated ANOVA, main effect of device, $F(1, 15) = 14.38, p=0.02$;
298 Figure 3B). The differences were greatest over the implant regions with bPVA-implanted retinas
299 having less GFAP immunoreactivity.

300 **4. Discussion**

301 The use of subretinal prostheses for the restoration of vision in patients with RP or AMD
302 depends upon an intact inner retina (O'Brien et al., 2012). Thus, it is critical that implantation of
303 a subretinal device does not cause a loss of inner retinal cells or excessive gliosis/fibrosis, as
304 both would interfere with the retinal-prosthesis interface. We have shown that a functional
305 connection that requires synaptic transmission within the inner retina drives PVA evoked
306 responses in the superior colliculus (Fransen et al., 2014). Here we show that the morphological
307 basis for this connectivity is an intact inner retina in subretinally-implanted m- and bPVA
308 devices. In addition, we show that morphology is maintained in two RP rat models, one with
309 direct photoreceptor degeneration, the other with RPE dysfunction induced photoreceptor
310 degeneration. This indicates that the effect we observe is general. We assessed rod bipolar
311 cells because they represent the primary transmission pathway from the PVA to the RGCs and
312 cholinergic amacrine cells because they are one of the most numerous amacrine cells and their
313 processes form well known sublaminae in the the IPL. Together the two measures provide a

314 general assessment of inner retinal cell organization. While it is well-established that the
315 degenerating retina undergoes remodeling when all photoreceptors are lost (Gargini et al.,
316 2007; Marc et al., 2003; Strettoi et al., 2002), we show that in these models, rod bipolar cells
317 and cholinergic amacrine cells within the implant site continue to exhibit typical and well-
318 preserved morphology. Both their somata and processes within the IPL show normal
319 localization and lamination. Previous studies show that normal retinas respond to both acute
320 epiretinal electrical stimulation (Ray et al., 2009; Ray et al., 2011), or chronic subretinal
321 implantation (Chow et al., 2001; Pardue et al., 2001; Tamaki et al., 2008; Yu et al., 2009) with
322 an upregulation of GFAP expression and degenerative changes to the dendrites of rod bipolar
323 cells. One study in which photosensitive dye-coupled film was subretinally implanted into RCS
324 rat eyes showed preservation within the implant site of rod bipolar cell morphology via PKC α
325 labeling (Alamusi et al., 2013), consistent with the findings we report here.

326 The increase in GFAP labeling in all unimplanted RCS and S334ter-3 retinas compared
327 to WT (images not shown) is consistent with previous reports on retinal remodeling during
328 degeneration (Marc and Jones, 2003; Zhao et al., 2012). Importantly, GFAP labeling in and
329 around the implant site was similar to distal areas, suggesting that the glial reaction was not
330 augmented by the presence of the PVA. Previous immunohistochemical studies of subretinal
331 implants in animals with normal retinas have shown an increase in GFAP expression within the
332 implant site (Chow et al., 2001; Pardue et al., 2001; Tamaki et al., 2008; Yu et al., 2009). It is
333 feasible that any upregulation in GFAP due to implantation is masked when extensive gliosis
334 due to photoreceptor degeneration is already present. Quantification of GFAP
335 immunofluorescence showed a significant decrease in S334ter-3 retinas implanted with bPVAs
336 compared to mPVAs. This may indicate that the gap design of the bPVA is more biocompatible
337 with the retina and reduces the stress response. As the PVA devices are active and present
338 electrical current to the underlying inner retina in response to light, it is possible that GFAP

339 expression in the Müller glia is tempered by neuroprotective effects of subretinal electrical
340 stimulation, which have been characterized previously (Ciavatta et al., 2013; Pardue et al.,
341 2005a; Pardue et al., 2005b).

342 The persistence of inner retinal cells and their intact organization under the implanted
343 device are consistent with our finding that PVA evoked responses are retained in the superior
344 colliculus and require inner retinal synaptic transmission (Fransen et al., 2014). Structural
345 integrity is critical to the success of function using this subretinal approach to visual restoration.
346 The presence of normal IPL sublamination suggests that other circuits that modulate the
347 excitatory signal are retained and may provide even better RGC and central signals. When
348 translated to the clinic, implantation will be performed at mid to late stage of photoreceptor
349 degeneration, similar to the implantation stages used here in the RCS and S334ter-3 rats,
350 respectively. The morphology of the retina implanted with both PVAs was similar, which also is
351 consistent with the functional results (Fransen et al., 2014) suggesting good compatibility at
352 both stages of degeneration.

353 The development of the next-generation bPVA is intended to improve upon the design of
354 the mPVA device, which has already been implanted in human patients (Chow et al., 2010;
355 Chow et al., 2004). Bipolar design of the pixel electrodes provides much tighter confinement of
356 electric field, and appears to improve spatial resolution, compared to monopolar arrangement in
357 mPVAs (Fransen et al., 2014). Our comparisons between mPVA- and bPVA-implanted retinas
358 and the reduced glial reaction in the retinas implanted with the bPVA device with the gaps
359 between pixels suggests improved biocompatibility and may indicate a longer duration of the
360 interface between the device and the retina, which needs to be tested empirically.

361 **5. Conclusions**

362 We found that both mPVA and bPVA devices implanted into the subretinal space were
 363 well tolerated by the inner retina in two rat models of RP with regard to rod bipolar, cholinergic
 364 amacrine, and Müller cell morphology. This initial analysis could be complemented with assays
 365 of other cell types (such as cone bipolar cells, horizontal cells as well as other amacrine cell
 366 classes). Other functional analyses could be aimed at examining the RGC responses and the
 367 timing and spatial distribution of their excitatory and inhibitory inputs. With our findings this
 368 would provide a complete understanding of the morphological and functional status of the inner
 369 retina in contact with the prosthesis.

370 **Acknowledgements**

371 Funding was provided by the National Institutes of Health (R01-EY-018608), the Air Force
 372 Office of Scientific Research (FA9550-04), NIH CTSA (UL1 RR025744, Stanford Spectrum
 373 fund) and a Stanford Bio-X IIP grant. K.M. was supported by an SU2P fellowship as part of an
 374 RCUK Science Bridges award. J.F. was supported by an NIH T32 grant (5 T32 HL 76138-09).
 375 M.P. was supported by a Research Career Scientist Award from the Department of Veterans
 376 Affairs.

377

378 **Table 1: Primary antibodies used in this study to characterize inner retinal health.**

Antigen	Antiserum	Source	Working Dilution	Cellular Target
PKC α	Polyclonal rabbit anti-PKC α	Santa Cruz Biotechnology, Inc., Dallas, TX	1:2000	Rod bipolar cells
GFAP	Polyclonal rabbit anti-GFAP	Abcam, Cambridge, MA	1:500	Glial reaction in retinal Müller cells
ChAT	Polyclonal goat anti-ChAT	Millipore, Billerica, MA	1:100	Cholinergic amacrine cells

379

380 **Figures Captions**

381 **Figure 1.** A) Sample fundus image of an RCS rat eye implanted subretinally with an mPVA.
382 White dotted line indicates location of the cut made in the superior to inferior plane bisecting the
383 posterior eye cup into implanted and non-implanted halves. “Implanted” region is indicated by
384 the blue line. The area immediately “adjacent” to the implant site is shown by the red line. The
385 green line displays an area opposite the implant within the non-implanted half, referred to as a
386 “distal” area. The implant is 1mm in diameter. PKC α labeling in retinal cross-sections from WT
387 rats (B), unimplanted control RCS rats at 2 months of age (F), RCS rats implanted from 4 to 8
388 weeks postnatal with a bPVA (C-E) and or mPVA (G-I). Rod bipolar cells are present with well-
389 preserved morphology and localization at the implant site (C and G) relative to adjacent (D and
390 H) and distal (E and I) regions. Implanted eyes show PKC α labeling consistent with that of age-
391 matched unimplanted RCS controls (F). Wild-type retinas (B) appear to exhibit more intact
392 dendritic tufts, but somata and axon terminal localization is comparable to that in RCS tissue.
393 Insets 1B, 1C, 1 F & 1G show magnified images of the dendritic tufts in the OPL. ONL=outer
394 nuclear layer, OPL=outer plexiform layer, INL=inner nuclear layer, IPL=inner plexiform layer,
395 GCL=ganglion cell layer. Scale bar=50 μ m.

396 **Figure 2.** PKC α labeling in retinal cross-sections from S334ter-3 rats implanted with a bPVA (B-
397 D, implanted from 7 to 27 weeks postnatal) or mPVA (F-H, implanted from 6 to 27 weeks
398 postnatal). Implanted sections (B and F) show rod bipolar cell morphology that is comparable to
399 that in adjacent (C and G) and distal (D and H) areas. The morphology and localization of these
400 sections is consistent with that seen in age-matched unimplanted S334ter-3 controls (E).
401 However, all S334ter-3 tissues exhibit virtually complete loss of the ONL and rod bipolar cell
402 dendrites, both of which are still evident in wild-type retina (A). Scale bar=50 μ m.

403 **Figure 3.** PKC α , GFAP, and ChAT labeling quantification. The relative length of PKC α -labeled
404 bipolar cells (A) did not show significant differences between retinal region or implant types. The

405 intensity of GFAP immunoreactivity (B) did not show significant differences between the retinal
406 location within each implant type, but did show a difference between implant types (Two-way
407 repeated ANOVA, $F(1, 15) = 14.38$ $p = 0.02$, $n = 6$). Immunoreactivity was normalized to the
408 distal position for the PKC α and GFAP labeling. ChAT immunoreactive cell counts did not show
409 significant differences between retinal location or implant type for either INL placed (C) or
410 displaced (D) cholinergic amacrine cells. Error bars represent standard error of the mean.

411 **Figure 4.** ChAT labeling in retinal cross-sections from RCS eyes (C-E, implanted from 4 to 8
412 weeks postnatal) and S334ter-3 eyes (G-I, implanted from 7 to 27 weeks postnatal) with bPVA
413 devices. Both RCS (B-E) and S334ter-3 sections (F-I), like wild-type (A), show typical
414 cholinergic amacrine cell morphology with somata in the INL and GCL and processes in a dual-
415 lamination pattern within the IPL. ChAT labeling patterns in implanted areas (C and G) are
416 identical to those in adjacent (D and H), distal (E and I), Scale bar=50 μ m.

417 **Figure 5.** ChAT-labeled retinal flat mounts from RCS rats implanted from 4 to 8 weeks postnatal
418 with an mPVA device (C and D) compared to unimplanted control eyes (A and B). *En face* view
419 of control INL placed (A) and implanted INL placed (C) ChAT positive amacrine cells shows
420 similar cholinergic amacrine cell distribution with consistent density. Similarly, labelling patterns
421 of ChAT positive amacrine cells in the ganglion cell layer were consistent between control (B)
422 and implanted (D) retinas. Scale bar=50 μ m.

423

424 **Figure 6.** GFAP labeling in retinal cross-sections from RCS (B-D) with bPVA and S334ter-3
425 eyes with mPVA (F-H) and bPVA (K-L) devices. RCS were implanted 4 to 8 weeks postnatally,
426 while the S334ter-3 animals were implanted at 12 to 32 weeks. Glial reaction is widespread in
427 all RCS tissue (A-D), but implanted areas (B) do not show increased GFAP labeling in
428 comparison with adjacent (C), distal (D), and age-matched unimplanted control (A) sections.
429 Similar to RCS tissue, S334ter-3 sections (E-L) show widespread gliosis due to photoreceptor

430 degeneration. However, GFAP labeling is not augmented in implanted regions (F and J) relative
431 to adjacent (G and K), distal (H and L), and age-matched unimplanted control section (E).
432 S334ter-3 retinas display a characteristic glial seal above the INL, not seen in wild-type retinas
433 (data not shown), consistent with advanced photoreceptor degeneration. NFL=nerve fiber layer.
434 Scale bar=50 μ m.

435

436

437

438

439

440

441

442

443

444

445

446

447

448

449

450

451

452

453

454

455

456 **References**

- 457 Adkins, A., Wang, W., Kaplan, H., Emery, D., Fernandez de Castro, J., Lee, S.-J., Huie, P.,
458 Palanker, D., McCall, M., Pardue, M., 2013. Morphological comparisons of flat and 3-
459 dimensional subretinal photovoltaic arrays in rat and pig models of retinitis pigmentosa.
460 Invest. Ophthalmol. Vis. Sci. 54, 1038.
- 461 Alamusi, Matsuo, T., Hosoya, O., Tsutsui, K.M., Uchida, T., 2013. Behavior tests and
462 immunohistochemical retinal response analyses in RCS rats with subretinal implantation
463 of Okayama-University-type retinal prosthesis. J. Artif. Organs 16, 343-351.
- 464 Asher, A., Segal, W.A., Baccus, S.A., Yaroslavsky, L.P., Palanker, D.V., 2007. Image
465 processing for a high-resolution optoelectronic retinal prosthesis. IEEE Trans. Biomed.
466 Eng. 54, 993-1004.
- 467 Bernstein, S.L., Guo, Y., 2011. Changes in cholinergic amacrine cells after rodent anterior
468 ischemic optic neuropathy (rAION). Invest. Ophthalmol. Vis. Sci. 52, 904-910.
- 469 Bi, A.D., Cui, J.J., Ma, Y.P., Olshevskaya, E., Pu, M.L., Dizhoor, A.M., Pan, Z.H., 2006. Ectopic
470 expression of a microbial-type rhodopsin restores visual responses in mice with
471 photoreceptor degeneration. Neuron 50, 23-33.
- 472 Bringmann, A., Pannicke, T., Grosche, J., Francke, M., Wiedemann, P., Skatchkov, S.N.,
473 Osborne, N.N., Reichenbach, A., 2006. Muller cells in the healthy and diseased retina.
474 Prog. Retin. Eye Res. 25, 397-424.
- 475 Busskamp, V., Picaud, S., Sahel, J.A., Roska, B., 2012. Optogenetic therapy for retinitis
476 pigmentosa. Gene Ther. 19, 169-175.
- 477 Chow, A.Y., Bittner, A.K., Pardue, M.T., 2010. The artificial silicon retina in retinitis pigmentosa
478 patients (an American Ophthalmological Association thesis). Trans. of the Am.
479 Ophthalmol. Soc. 108, 120-154.

480 Chow, A.Y., Chow, V.Y., Packo, K.H., Pollack, J.S., Peyman, G.A., Schuchard, R., 2004. The
481 artificial silicon retina microchip for the treatment of vision loss from retinitis pigmentosa.
482 Arch. Ophthalmol. 122, 460-469.

483 Chow, A.Y., Pardue, M.T., Chow, V.Y., Peyman, G.A., Liang, C., Perlman, J.I., Peachey, N.S.,
484 2001. Implantation of silicon chip microphotodiode arrays into the cat subretinal space.
485 IEEE Trans. Neural Syst. Rehabil. Eng. 9, 86-95.

486 Ciavatta, V.T., Mocko, J.A., Kim, M.K., Pardue, M.T., 2013. Subretinal electrical stimulation
487 preserves inner retinal function in RCS rat retina. Mol. Vis. 19, 995-1005.

488 Cicione, R., Shivdasani, M.N., Fallon, J.B., Luu, C.D., Allen, P.J., Rathbone, G.D., Shepherd,
489 R.K., Williams, C.E., 2012. Visual cortex responses to suprachoroidal electrical
490 stimulation of the retina: effects of electrode return configuration. J. Neural Eng. 9,
491 036009.

492 Dijk, F., Kamphuis, W., 2004. An immunocytochemical study on specific amacrine cell
493 subpopulations in the rat retina after ischemia. Brain Res. 1026, 205-217.

494 Fransen, J. W., Pangeni, G., Pardue, M.T., McCall, M.A. 2014. Local signaling from a retinal
495 prosthetic in a rodent retinitis pigmentosa model in vivo. J. Neural Eng. 11, 046012.

496 Garg, S.J., Federman, J., 2013. Optogenetics, visual prosthesis and electrostimulation for
497 retinal dystrophies. Curr. Opin. Ophthalmol. 24, 407-414.

498 Gargini, C., Terzibasi, E., Mazzoni, F., Strettoi, E., 2007. Retinal organization in the retinal
499 degeneration 10 (rd10) mutant mouse: a morphological and ERG study. J. Comp.
500 Neurol. 500, 222-238.

501 Grünert, U., Martin, P.R., 1991. Rod bipolar cells in the macaque monkey retina:
502 immunoreactivity and connectivity. J Neurosci. 11, 2742-2758.

503 Hartong, D.T., Berson, E.L., Dryja, T.P., 2006. Retinitis pigmentosa. Lancet 368, 1795-1809.

504 Humayun, M.S., Dorn, J.D., da Cruz, L., Dagnelie, G., Sahel, J.A., Stanga, P.E., Cideciyan,
505 A.V., Duncan, J.L., Elliott, D., Filley, E., Ho, A.C., Santos, A., Safran, A.B., Arditi, A., Del

506 Priore, L.V., Greenberg, R.J., Argus, I.I.S.G., 2012. Interim results from the international
507 trial of Second Sight's visual prosthesis. *Ophthalmology* 119, 779-788.

508 Humayun, M.S., Prince, M., de Juan, E., Barron, Y., Moskowitz, M., Klock, I.B., Milam, A.H.,
509 1999. Morphometric analysis of the extramacular retina from postmortem eyes with
510 retinitis pigmentosa. *Invest. Ophthalmol. Vis. Sci.* 40, 143-148.

511 Isago, H., Sugano, E., Wang, Z., Murayama, N., Koyanagi, E., Tamai, M., Tomita, H., 2012.
512 Age-Dependent Differences in Recovered Visual Responses in Royal College of
513 Surgeons Rats Transduced with the Channelrhodopsin-2 Gene. *J. of Mol. Neurosci.* 46,
514 393-400.

515 Jensen, R.J., Ziv, O.R., Rizzo, J.F., 2005. Responses of rabbit retinal ganglion cells to electrical
516 stimulation with an epiretinal electrode. *J. Neural Eng.* 2, S16-21.

517 Jones, B.W., Watt, C.B., Frederick, J.M., Baehr, W., Chen, C.K., Levine, E.M., Milam, A.H.,
518 Lavail, M.M., Marc, R.E., 2003. Retinal remodeling triggered by photoreceptor
519 degenerations. *J. Comp. Neurol.* 464, 1-16.

520 Jones, B.W., Marc, R.E., 2005. Retinal remodeling during retinal degeneration. *Exp. Eye Res.*
521 81, 123-137.

522 Kanda, H., Morimoto, T., Fujikado, T., Tano, Y., Fukuda, Y., Sawai, H., 2004.
523 Electrophysiological studies of the feasibility of suprachoroidal-transretinal stimulation for
524 artificial vision in normal and RCS rats. *Invest. Ophthalmol. Vis. Sci.* 45, 560-566.

525 Kosaka, J., Suzuki, A., Morii, E., Nomura, S., 1998. Differential localization and expression of
526 alpha and beta isoenzymes of protein kinase C in the rat retina. *J. Neurosci. Res.* 54,
527 655-663.

528 LaVail, M.M., Battelle, B.A., 1975. Influence of eye pigmentation and light deprivation on
529 inherited retinal dystrophy in the rat. *Exp. Eye Res.* 21, 167-192.

530 LaVail, M.M., Sidman, R.L., Gerhardt, C.O., 1975. Congenic strains of RCS rats with inherited
531 retinal dystrophy. *J. Hered.* 66, 242-244.

532 Lee, E.J., Padilla, M., Merwine, D.K., Grzywacz, N.M., 2008. Developmental regulation of the
533 morphology of mouse retinal horizontal cells by visual experience. *Eur. J. Neurosci.* 27,
534 1423-1431.

535 Lin, B., Koizumi, A., Tanaka, N., Panda, S., Masland, R.H., 2008. Restoration of visual function
536 in retinal degeneration mice by ectopic expression of melanopsin. *Proc. Natl. Acad. Sci.*
537 U.S.A. 105, 16009-16014.

538 Mandel, Y., Goetz, G., Lavinsky, D., Huie, P., Mathieson, K., Wang, L., Kamins, T., Galambos,
539 L., Manivanh, R., Harris, J., Palanker, D., 2013. Cortical responses elicited by
540 photovoltaic subretinal prostheses exhibit similarities to visually evoked potentials. *Nat.*
541 *Commun.* 4, 1980.

542 Marc, R.E., Jones, B.W., 2003. Retinal remodeling in inherited photoreceptor degenerations.
543 *Mol. Neurobiol.* 28, 139-147.

544 Marc, R.E., Jones, B.W., Anderson, J.R., Kinard, K., Marshak, D.W., Wilson, J.H., Wensel, T.,
545 Lucas, R.J., 2007. Neural reprogramming in retinal degeneration. *Invest. Ophthalmol.*
546 *Vis. Sci.* 48, 3364-3371.

547 Marc, R.E., Jones, B.W., Watt, C.B., Strettoi, E., 2003. Neural remodeling in retinal
548 degeneration. *Prog. Retin. Eye Res.* 22, 607-655.

549 Mathieson, K., Loudin, J., Goetz, G., Huie, P., Wang, L., Kamins, T.I., Galambos, L., Smith, R.,
550 Harris, J.S., Sher, A., Palanker, D., 2012. Photovoltaic Retinal Prosthesis with High Pixel
551 Density. *Nat. Photonics* 6, 391-397.

552 McGill, T.J., Prusky, G.T., Douglas, R.M., Yasumura, D., Matthes, M.T., Lowe, R.J., Duncan,
553 J.L., Yang, H., Ahern, K., Daniello, K.M., Silver, B., LaVail, M.M., 2012. Discordant
554 anatomical, electrophysiological, and visual behavioral profiles of retinal degeneration in
555 rat models of retinal degenerative disease. *Invest. Ophthalmol. Vis. Sci.* 53, 6232-6244.

556 Morimoto, T., Kamei, M., Nishida, K., Sakaguchi, H., Kanda, H., Ikuno, Y., Kishima, H., Maruo,
557 T., Konoma, K., Ozawa, M., Nishida, K., Fujikado, T., 2011. Chronic Implantation of

558 Newly Developed Suprachoroidal-Transretinal Stimulation Prosthesis in Dogs. Invest.
559 Ophthalmol. Vis. Sci. 52, 6785-6792.

560 Mullen, R.J., LaVail, M.M., 1976. Inherited retinal dystrophy: primary defect in pigment
561 epithelium determined with experimental rat chimeras. Science 192, 799-801.

562 O'Brien, E.E., Greferath, U., Vessey, K.A., Jobling, A.I., Fletcher, E.L., 2012. Electronic
563 restoration of vision in those with photoreceptor degenerations. Clin. Exp. Optom. 95,
564 473-483.

565 Palanker, D., Huie, P., Vankov, A., Aramant, R., Seiler, M., Fishman, H., Marmor, M.,
566 Blumenkranz, M., 2004. Migration of retinal cells through a perforated membrane:
567 implications for a high-resolution prosthesis. Invest. Ophthalmol. Vis. Sci. 45, 3266-3270.

568 Pardue, M.T., Phillips, M.J., Yin, H., Fernandes, A., Cheng, Y., Chow, A.Y., Ball, S.L., 2005a.
569 Possible sources of neuroprotection following subretinal silicon chip implantation in RCS
570 rats. J. Neural Eng. 2, S39-47.

571 Pardue, M.T., Phillips, M.J., Yin, H., Sippy, B.D., Webb-Wood, S., Chow, A.Y., Ball, S.L., 2005b.
572 Neuroprotective effect of subretinal implants in the RCS rat. Invest. Ophthalmol. Vis. Sci.
573 46, 674-682.

574 Pardue, M.T., Stubbs, E.B., Jr., Perlman, J.I., Narfstrom, K., Chow, A.Y., Peachey, N.S., 2001.
575 Immunohistochemical studies of the retina following long-term implantation with
576 subretinal microphotodiode arrays. Exp. Eye Res. 73, 333-343.

577 Ray, A., Colodetti, L., Weiland, J.D., Hinton, D.R., Humayun, M.S., Lee, E.J., 2009.
578 Immunocytochemical analysis of retinal neurons under electrical stimulation. Brain Res.
579 1255, 89-97.

580 Ray, A., Lee, E.J., Humayun, M.S., Weiland, J.D., 2011. Continuous electrical stimulation
581 decreases retinal excitability but does not alter retinal morphology. J. Neural Eng. 8,
582 045003.

583 Rizzo, J.F., 3rd, 2011. Update on retinal prosthetic research: the Boston Retinal Implant Project.
584 J. Neuroophthalmol. 31, 160-168.

585 Strettoi, E., Porciatti, V., Falsini, B., Pignatelli, V., Rossi, C., 2002. Morphological and functional
586 abnormalities in the inner retina of the rd/rd mouse. J. Neurosci. 22, 5492-5504.

587 Strettoi, E., Pignatelli, V., Rossi, C., Porciatti, V., Falsini, B., 2003. Remodeling of second-order
588 neurons in the retina of rd/rd mutant mice. Vision Research 43, 867–877.

589 Tamaki, T., Matsuo, T., Hosoya, O., Tsutsui, K.M., Uchida, T., Okamoto, K., Uji, A., Ohtsuki, H.,
590 2008. Glial reaction to photoelectric dye-based retinal prostheses implanted in the
591 subretinal space of rats. J. Artif. Organs 11, 38-44.

592 Tomita, H., Sugano, E., Yawo, H., Ishizuka, T., Isago, H., Narikawa, S., Kugler, S., Tamai, M.,
593 2007. Restoration of visual response in aged dystrophic RCS rats using AAV-mediated
594 channelopsin-2 gene transfer. Invest. Ophthalmol. Vis. Sci. 48, 3821-3826.

595 Uji, A., Matsuo, T., Ishimaru, S., Kajiura, A., Shimamura, K., Ohtsuki, H., Dan-oh, Y., Suga, S.,
596 2005. Photoelectric dye-coupled polyethylene film as a prototype of retinal prostheses.
597 Artif. Organs 29, 53-57.

598 Wang, L., Mathieson, K., Kamins, T.I., Loudin, J.D., Galambos, L., Goetz, G., Sher, A., Mandel,
599 Y., Huie, P., Lavinsky, D., Harris, J.S., Palanker, D.V., 2012. Photovoltaic retinal
600 prosthesis: implant fabrication and performance. J. Neural Eng. 9, 046014.

601 Wong, Y.T., Chen, S.C., Seo, J.M., Morley, J.W., Lovell, N.H., Suaning, G.J., 2009. Focal
602 activation of the feline retina via a suprachoroidal electrode array. Vis. Res. 49, 825-833.

603 Yamauchi, Y., Franco, L.M., Jackson, D.J., Naber, J.F., Ziv, R.O., Rizzo, J.F., Kaplan, H.J.,
604 Enzmann, V., 2005. Comparison of electrically evoked cortical potential thresholds
605 generated with subretinal or suprachoroidal placement of a microelectrode array in the
606 rabbit. J. Neural Eng. 2, S48-56.

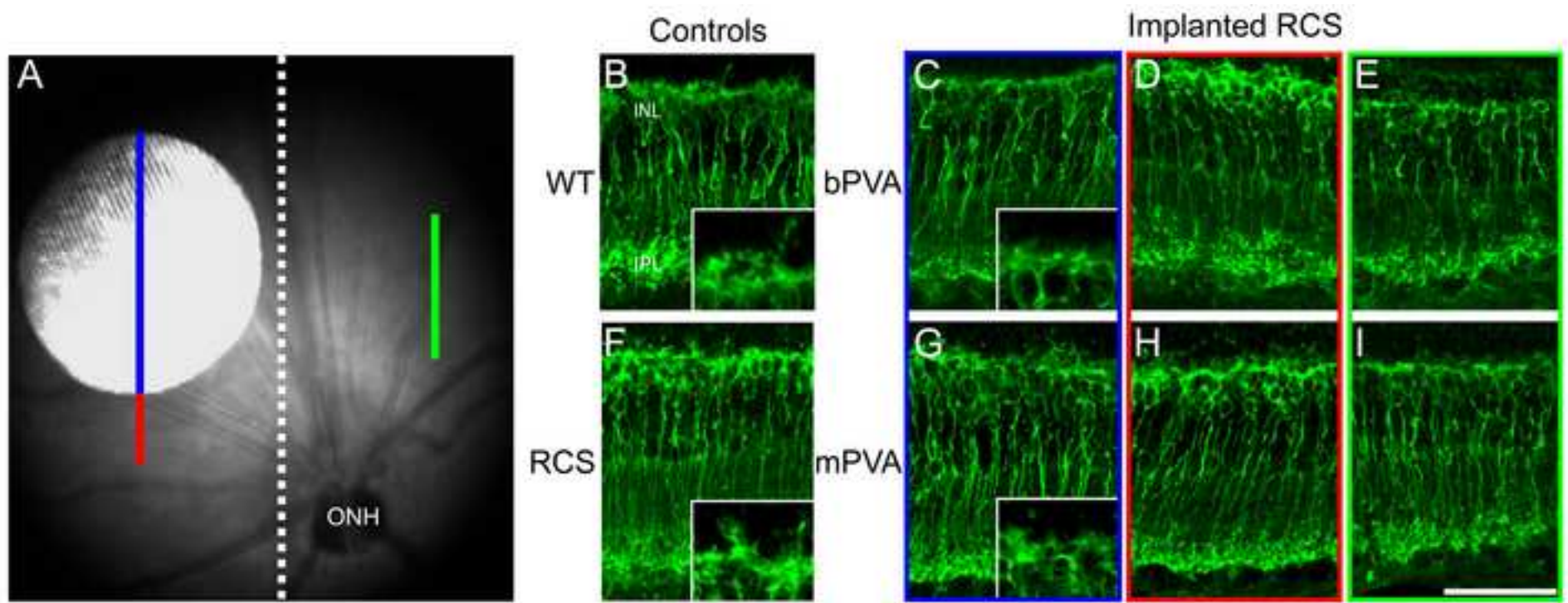
607 Yu, W., Wang, X., Zhao, C., Yang, Z., Dai, R., Dong, F., 2009. Biocompatibility of subretinal
608 parylene-based Ti/Pt microelectrode array in rabbit for further artificial vision studies. *J.*
609 *Ocul. Biol. Dis. Infor.* 2, 33-36.

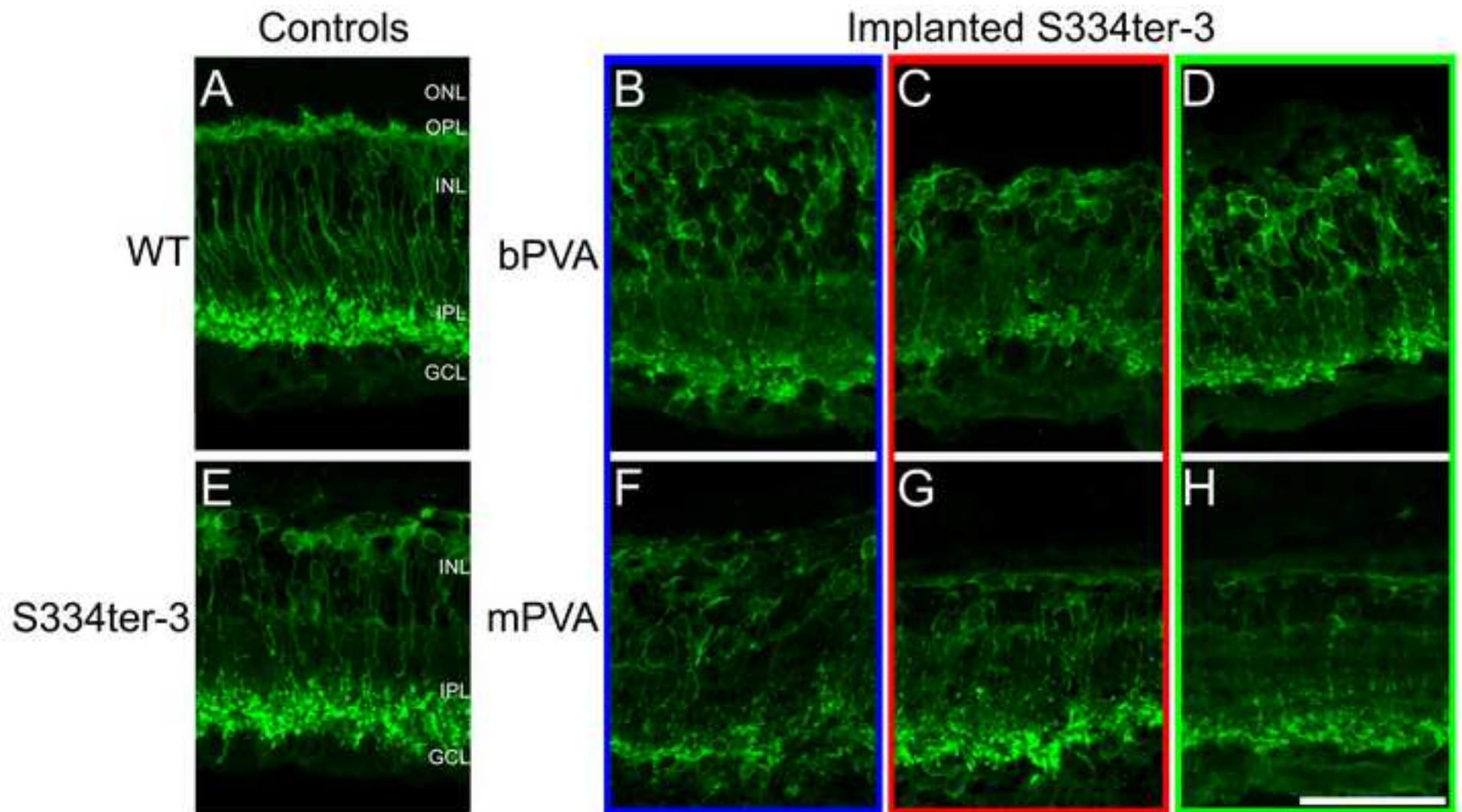
610 Zhao, T., Li, Y., Weng, C., Yin, Z., 2012. The changes of potassium currents in RCS rat Muller
611 cell during retinal degeneration. *Brain Res.* 1427, 78-87.

612 Zrenner, E., Stett, A., Weiss, S., Aramant, R.B., Guenther, E., Kohler, K., Miliczek, K.D., Seiler,
613 M.J., Haemmerle, H., 1999. Can subretinal microphotodiodes successfully replace
614 degenerated photoreceptors? *Vis. Res.* 39, 2555-2567.

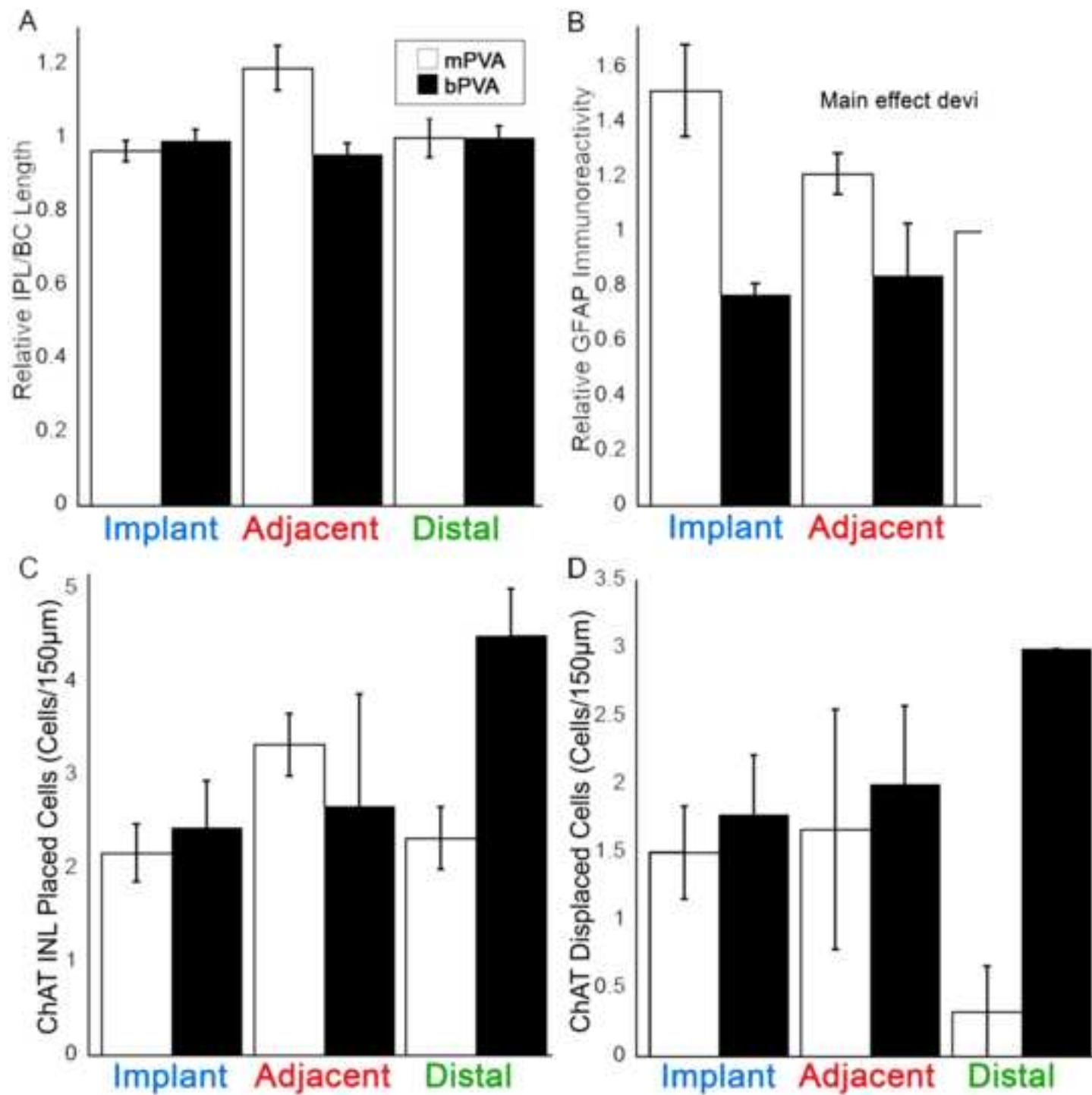
615

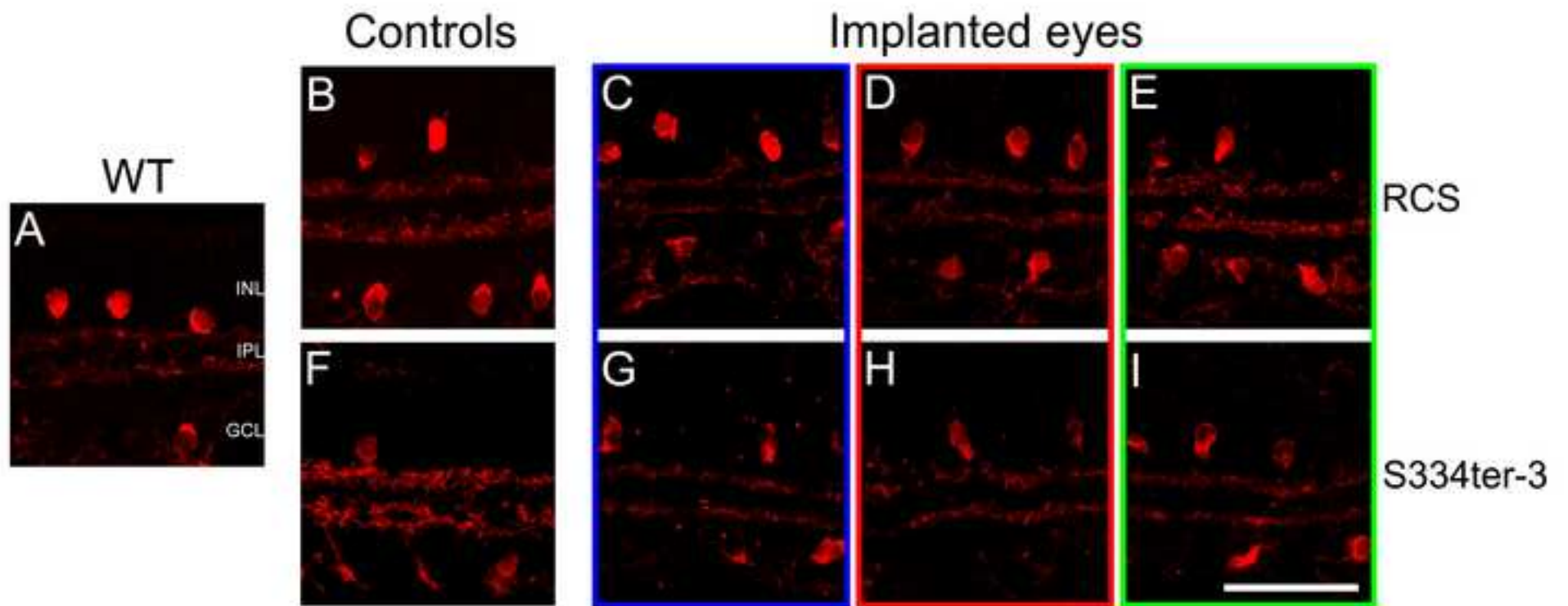
616

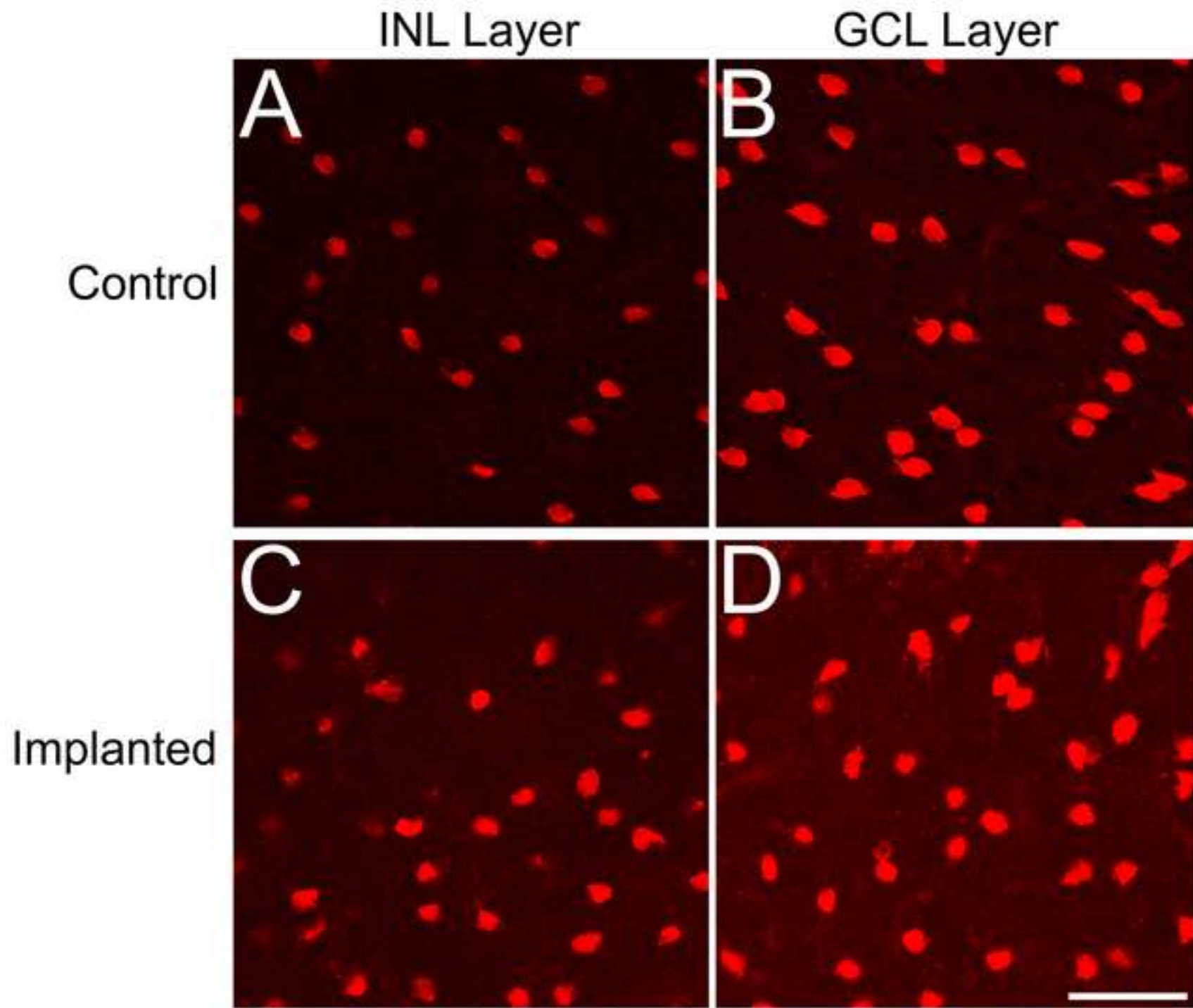




Figure(s)
[Click here to download high resolution image](#)







Figure(s)
[Click here to download high resolution image](#)

